### Title

Effective drug and shRNA delivery for synergistic treatment of triple-negative breast cancer by sequentially targeting tumor hypoxia




### Authors

Liu, Xuemeng

Sun, Jiajia

Gu, Jia

et al.



### Publication Date

2023-08-01

### DOI

10.1016/j.cej.2023.144271

Chemical Engineering Journal 470 (2023) 144271

Contents lists available at ScienceDirect

Chemical Engineering Journal

journal homepage: www.elsevier.com/locate/cej

# Effective drug and shRNA delivery for synergistic treatment of triple-negative breast cancer by sequentially targeting tumor hypoxia

Xuemeng Liu [1], Jiajia Sun [1], Jia Gu, Lingyan Weng, Xueting Wang, Li Zhu [*], Qianqian Luo [*], Zhongping Chen [*]

*Institute of Special Environmental Medicine and Co-innovation Center of Neuroregeneration, Nantong University, Nantong 226019, People's Republic of China*

ARTICLE INFO

*Keywords:*
Polymeric micelles
Tumor hypoxia
Hypoxia-responsive
Drug delivery
shRNA delivery
Triple-negative breast cancer

ABSTRACT

Clinical treatment of TNBC remains challenging, due to the lack of targeted therapies. As TNBC is highly hypoxic with higher HIF-1α expression than other subtypes, we fabricated hypoxia-responsive polymeric micelles co-loading drug and shRNA to treat TNBC by targeting hypoxic tumor microenvironment and subsequently targeting overexpressed HIF-1α under hypoxia. The micelles were assembled from methoxy-polyethylene glycol (mPEG) and poly-*L*-lysine (PLL) copolymer with AZO as a hypoxia-responsive bridge of mPEG and PLL. Once exposed to hypoxia, AZO bridge was cleaved, resulting in the disassembly of the micelles for rapid release. *In vitro* and *in vivo* results showed that the micelles enabled simultaneous delivery of drug and shRNA to hypoxic sites for site-specific rapid release, facilitated by sensitive response to hypoxia; hypoxia-responsive shRNA delivery effectively silenced HIF-1α and its downstream genes, which not only ameliorated the response of hypoxic tumor to drug, but also modulated tumor microenvironment for further improved drug and shRNA delivery; as a result, synergistic treatment of chemotherapy and HIF-1α targeted gene therapy inhibited the growth of primary TNBC tumor and its distant metastasis in a murine model of orthotopic TNBC. Together with their good biocompatibility, hypoxia-responsive polymeric micelles thus emerged as a safe, effective, and universally applicable drug and gene carrier for treatment of TNBC as well as other hypoxic tumors.

## 1. Introduction

Cancer represents a serious threat to public health and life. For women, breast cancer (BC) accounts for 30% of all newly diagnosed cancer and 15% of cancer-related death annually, ranking 1st in incidence and 2rd in mortality globally, respectively [1,2]. Thanks to remarkable progress in cancer screening and management, BC generally has a good prognosis and survival rate. Triple-negative breast cancer (TNBC) is a special subtype of BC, which lacks the expression of estrogen receptor (ER), progesterone receptor (PR), and human epidermal growth factor receptor (HER-2). Compared with other types and subtypes of BC, TNBC patients have a short median survival time of only 13.3 months [3] and a high mortality rate of more than 50% within 5 years after diagnosis [4]. Moreover, TNBC is highly invasive and almost half of TNBC patients will experience distant metastasis, portending the worst prognosis. Due to its special molecular phenotype, there is still no molecular targeted therapy available for TNBC [5]. Therefore, cytotoxic chemotherapy using taxanes, anthracyclines, cyclophosphamide, platinum agents, fluorouracil, or their combinations is currently the only systemic treatment regimen for TNBC. However, its therapeutic outcome is far from satisfactory. TNBC patients not only suffer from serious systemic toxicity, due to high-frequency and high-dose regimen, but also risk locoregional recurrence and distant metastasis following treatment [6]. In some cases, chemotherapy even promotes TNBC metastasis by activating specific signal pathways [7].

With continued advancements in understanding tumor biology, it is accepted that as an indispensable component of tumor tissue functioning as the soil for tumor cells, tumor microenvironment (TME) poses a formidable obstacle to chemotherapy and other therapies. TME is characterized by abnormal tumor vasculature, high interstitial pressure, abundant stroma cells, and dense extracellular matrix, resulting in ineffective drug transport to tumor sites, confined interstitial transport within tumor, and limited uptake by tumor cells, consequently contributing to therapeutic failure [8,9]. Altering feature and

* Corresponding authors.
*E-mail addresses:* zhulizhou@ntu.edu.cn (L. Zhu), qianqianluo@ntu.edu.cn (Q. Luo), chenzp@ntu.edu.cn (Z. Chen).
[1] These authors contributed equally to this work.

https://doi.org/10.1016/j.cej.2023.144271
Received 11 January 2023; Received in revised form 8 June 2023; Accepted 19 June 2023
Available online 22 June 2023

composition of TME using TME modulators that can modulate tumor vasculature, extracellular matrix, and stroma cells can improve drug extravasation and interstitial transport as well as reduce off-target uptake by immune cells, ultimately benefiting chemotherapy and other therapies [9,10]. Unfortunately, few of them have displayed positive results in early clinical trials, due to the heterogeneity, complexity, and interconnection of TME. In recent decades, nanoparticle-based drug delivery system (NDDS) has been extensively developed to facilitate drug delivery, achieved by improved pharmacokinetic performances, passive drug accumulation through the enhanced permeability and retention (EPR) effect, and nanoparticle-mediated tumor penetration and cell uptake [11–13]. However, the outstanding clinical benefit of NDDS seems to be reduced systemic toxicity. For example, albumin bound paclitaxel (Abraxane) and PEGylated liposomal doxorubicin (Doxil) only display a modest outcome in clinical cancer treatment when compared with carrier-free formulations [14]. NDDS is also developed as gene carrier for gene therapy to combat cancer including TNBC by specifically regulating genes implicated in pathogenesis to produce a positive therapeutic effect [15,16]. However, effective *in vivo* gene delivery remains challenging, which has hampered clinical translation. Delivery obstacle posed by TME might still be the main reason for unsatisfactory therapeutic outcome of conventional NDDS. Smart stimuli-responsive NDDS that can respond to the intrinsic stimuli from TME, such as acidic pH, high redox, and overexpressed enzyme, enabling effective drug and gene delivery to tumor sites, are thus developed [17,18].

Hypoxia is a prevalent feature of TME, as a result of improper balance between insufficient oxygen supply and rapid oxygen consumption. Hypoxia-inducible factor 1 (HIF-1) pathway is activated under hypoxia and HIF-1α, oxygen-labile α subunit, is stabilized and overexpressed, enabling tumor cells to adapt to this harsh condition. It has been widely evidenced that overexpression of HIF-1α induces a more invasive and metastatic phenotype by promoting epithelial-mesenchymal transition or activating its downstream pathways involved in tumor angiogenesis, invasiveness, metastasis, and therapeutic resistance. Thereby, overexpressed HIF-1α is considered as a reverse indicator of tumor prognosis. On the other hand, given its functions in tumor progression, HIF-1α emerges as a therapeutic target with more than 100 clinical trials testing HIF-1α inhibitors as antitumor agents [19].

Hypoxic TME causes a high reductive stress with overexpression of some reductases, such as nitro and azo reductases, which triggers the development of hypoxia-responsive NDDS with decorated hypoxia-responsive moieties, such as nitroimidazoles and azo compound (AZO) [20]. Our previous work validated that hypoxia-responsive NDDS was capable of crossing TME and delivering its payload to hypoxic sites through the process of stimulating, responding, disassembling, and releasing, maximizing enhanced therapeutic outcome *in vitro* and *in vivo* [21–24]. Especially, hypoxia-responsive NDDS could specifically release its payload to where HIF-1α was overexpressed [21]. Therefore, it is hypothesized that hypoxia-responsive NDDS is particularly valuable in HIF-1α targeted cancer therapy. TNBC is highly hypoxic with higher HIF-1α expression than other BC subtypes. Moreover, it is found that HIF-1α regulates the complex biological process of TNBC, such as glycolysis, angiogenesis, invasion, metastasis, and immune escape, driving TNBC progression [25]. Therefore, targeting hypoxic TME and targeting HIF-1α are of great significance in TNBC treatment. We herein fabricated hypoxia-responsive polymeric micelles co-loading doxorubicin (DOX) and short hairpin RNA (shRNA) that specifically targets HIF-1α (shHIF-1α) for synergistic chemotherapy and gene therapy of

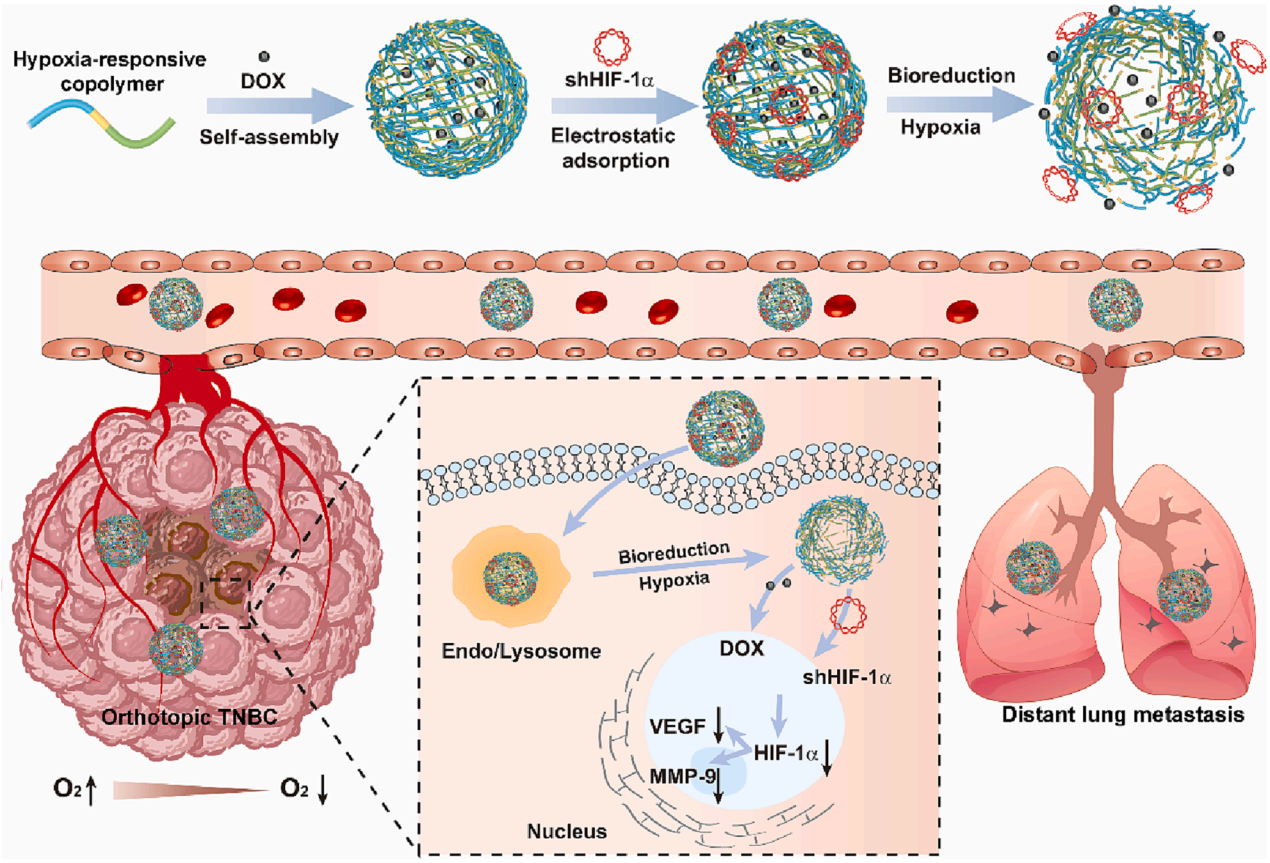


**Scheme 1.** Hypoxia-responsive micelles co-loading DOX and shHIF-1α for synergistic chemotherapy and gene therapy of TNBC by targeting hypoxic TME and targeting activated HIF-1α pathway under hypoxia. The micelles were self-assembled from the copolymer composed of mPEG (blue segment) and PLL (green segment) with AZO (yellow segment) as a hypoxia-responsive bridge.

TNBC by sequentially targeting tumor hypoxia. It was expected that hypoxia-responsive micelles could greatly facilitate DOX and shHIF-1α delivery through sensitive response to hypoxia and subsequently effectively silence overexpressed HIF-1α and its activated downstream genes under hypoxia. Consequently, the micelles could modulate hypoxic TME and maximize therapeutic outcome of DOX, inhibiting the growth of primary TNBC tumor and its distant metastasis (Scheme 1).

## 2. Materials and methods

### 2.1. Chemical agents

Methoxy-polyethylene glycol-amine (mPEG-$NH_2$, $M_w$ = 2000) and methoxy-polyethylene glycol-N-hydroxysuccinimide (mPEG-NHS, $M_w$ = 2000) were purchased from ToYongBio Tech. Inc. (Shanghai, China). Sodium dithionite ($Na_2S_2O_4$), 4, 4′-azodiphenylamine (azo compound, AZO), and doxorubicin hydrochloride (DOX·HCl) were obtained from J&K Scientific LTD (Beijing, China). shRNA plasmid was purchased from Gemma Gene (Shanghai, China). Lipofectamine 2000 was obtained from Glpbio (CA, USA). All other chemicals were from Sinopharm Chemical Reagent CO., LTD. (Shanghai, China). All reagents were of analytical grade and used as received. Millipore water was used in all experiments unless otherwise indicated.

### 2.2. Synthetic procedures

#### 2.2.1. Copolymer synthesis

Hypoxia-responsive copolymer composed of mPEG, AZO, and PLL (mPEG-AZO-PLL) as well as non-responsive copolymer (mPEG-PLL) was synthesized according to our previous work with a minor modification [23]. The structure of mPEG-AZO-PLL and mPEG-PLL was verified by $^1$H NMR spectra recorded on a 400 MHz NMR spectrometer (Avance III, Bruker) using C*D*$Cl_3$ as solvent.

#### 2.2.2. Synthesis of blank and DOX-loaded polymeric micelles

mPEG-PLL and mPEG-AZO-PLL copolymers were used to synthesize non-responsive and hypoxia-responsive polymeric micelles (PMs and AZO-PMs), respectively, via self-assembly technique. In a typical experiment for the synthesis of AZO-PMs, 20 mg of mPEG-AZO-PLL was dissolved in 2 mL of DMSO and 10 mL of water was added drop by drop with vigorous stirring. The mixture was then dialyzed against water (MWCO = 14000) for 24 h to produce blank AZO-PMs.

To improve loading efficiency, hydrophilic DOX·HCl was desalted and obtained hydrophobic DOX was mixed with mPEG-PLL and mPEG-AZO-PLL in DMSO to synthesize PMs/DOX and AZO-PMs/DOX, respectively, according to the above-described protocol. Micelles in suspension could be quantified by lyophilization.

#### 2.2.3. Synthesis of DOX and shRNA co-loaded polymeric micelles

Negatively charged shRNA was bound to positively charged micelles through electrostatic adsorption. In a typical experiment, 1 μg of shHIF-1α plasmid was mixed with 15 μg of AZO-PMs/DOX and the mixture was slightly shaken for 30 min to produce DOX and shHIF-1α co-loaded micelles (AZO-PMs/DOX + shHIF-1α). Similarly, shHIF-1α alone was bound to blank micelles, producing PMs/shHIF-1α or AZO-PMs/shHIF-1α.

### 2.3. Characterization

#### 2.3.1. Gel retardation assay

The binding of shHIF-1α with micelles was verified by agarose gel electrophoresis. Synthesized shHIF-1α loaded micelles through above-described protocol were loaded onto 1% agarose gel and electrophoresis was performed in TBE buffer solution at 100 mV for 30 min. The retardation of shHIF-1α was observed under UV light on a gel imaging system (Tanon-4100, China). The ratio of shHIF-1α to micelles was varied (1:1, 1:4, 1:10, 1:15, 1:20, and 1:50, shHIF-1α/micelles, w/w) to optimize shHIF-1α binding. The amount of shHIF-1α was fixed at 1 μg. In another experiment, shHIF-1α loaded micelles were incubated in PBS (pH 7.4) containing 50% fetal bovine serum (FBS) at 37 °C and at the predetermined intervals (0, 2, 4, 6, 12, 24, 36, and 48 h), the retardation of shHIF-1α was studied to evaluate serum stability of shHIF-1α loaded micelles.

#### 2.3.2. Size, surface charge, and morphology

The size and morphology of micelles were observed on a transmission electron microscope (TEM, JEM-1230, Japan). Hydrodynamic diameter, polydispersity index (PDI), and zeta potential of micelles were investigated by dynamic light scattering technique (DLS, Zetasizer ZS90, Malvern).

#### 2.3.3. Drug loading

Drug entrapment efficiency (EE%) and loading capacity (LC%) of micelles were determined by fluorescence method. Briefly, 100 μL of DOX-loaded micelle suspension was added into 4.9 mL of methanol solution. An ultrasonic cell pulverizer was then used to completely rupture the micelles to release loaded DOX. Followed by centrifugation at 5600 g for 10 min, the supernatant was collected and fluorescence emission spectrum of DOX was recorded on a fluorescence spectrophotometer (CTO-10AS, SHIMADZU, Japan). DOX was quantified based on a pre-established standard curve by plotting emission intensity (excitation wavelength = 488 nm and emission wavelength = 560 nm) against DOX concentrations ($y = 122.14x + 31.4$, $R^2 = 0.9994$). EE% was defined as loaded DOX relative to initially added DOX (w/w), while LC% was defined as loaded DOX relative to DOX-loaded micelles (w/w).

#### 2.3.4. In vitro response to hypoxia

A chemical hypoxia (2 mg of $Na_2S_2O_4$ in 2 mL of water) was generated to mimic hypoxic TME. One milligram of blank micelles was added into above hypoxic solution and sealed in a quartz cuvette for 12 h. The changes in characteristic peaks before and after hypoxic treatment were recorded to study *in vitro* response to hypoxia on a UV–vis spectrophotometer (UV-2401PC, Shimadzu).

#### 2.3.5. In vitro hypoxia-responsive release

The method described in section 2.3.4 was also carried out to study hypoxia-responsive DOX release. In a typical experiment, 1 mg of AZO-PMs/DOX added into the hypoxic solution was transferred into a dialysis bag (MWCO = 14000) and then dispersed in 30 mL of degassed PBS as release medium with gentle stirring at 37 °C. $N_2$ was bubbled into the medium throughout the experiment. At the predetermined intervals (0.5, 1, 2, 4, 6, 12 and 24 h), 1 mL aliquot of the dialysate containing released DOX was withdrawn with equivalent fresh PBS added immediately. DOX in the dialysate was quantified based on the pre-established standard curve using fluorescence spectrophotometer. A cumulative release curve was obtained by plotting cumulative released DOX percentage against time.

Hypoxia-responsive shHIF-1α release was studied by gel retardation assay. In a typical experiment, 10 μg of AZO-PMs/DOX + shHIF-1α was added into the hypoxic solution and following the incubation for 4 h, the solution was loaded onto 1% agarose gel for agarose gel electrophoresis, as described in section 2.3.1.

### 2.4. Cell experiments

#### 2.4.1. Cell culture

Human embryonic kidney cells (HEK-293 T) and human triple-negative breast cancer cells (MDA-MB-231) were obtained from Cell Resource Center of Institute of Biological Sciences, Chinese Academy of Sciences (Shanghai, China). MDA-MB-231 and HEK-293 T cells were cultured in Leibovitz's L-15 medium with L-glutamine (37℃, 100% air atmosphere) and Dulbecco's modified eagle's medium (DMEM) (37℃,

5% $CO_2$ atmosphere), respectively, containing 10% FBS and 1% penicillin/streptomycin.

#### 2.4.2. Construction and efficiency validation of shRNA

shHIF-1α targeting human HIF-1α mRNA was designed and constructed by Genepharma (Shanghai, China). To get shHIF-1α with high efficiency, different target sequences were designed (shHIF-1α-934, shHIF-1α-1405, shHIF-1α-1067, and shHIF-1α-2637), which was summarized in Supplementary Table S1. A scrambled non-silencing shRNA (shNC) was designed as a negative control. The shRNA sequences were integrated into pGPU6/GFP/Neo plasmid and then transfected into HEK-293 T cells using lipofectamine 2000, according to manufacturer's protocol, to assess transfection efficiency. The silencing efficiency was further validated by western blot and quantitative reverse transcription PCR (RT-qPCR) with the protocol described below.

#### 2.4.3. Intracellular hypoxia-responsive release

Hypoxia-responsive release was studied in 2D-cultured cell monolayers and 3D-cultured cell spheroids. General treatment protocols for cell monolayers were as follows: MDA-MB-231 cells ($2 \times 10^5$) cultured under normoxia were treated with different drug formulations (0.5 μg/mL DOX or its equal volume) and subsequently incubated for 4 h under normoxia for cell uptake. After washing twice with PBS to remove uninternalized formulations, the cells were subjected to normoxia, fixed hypoxia (1% $O_2$), or gradient hypoxia for another 24 h for further analysis. The fixed hypoxia was generated by a hypoxia incubator using a hypoxia workstation ((INVIVO2, Ruskinn); the gradient hypoxia was induced by placing a coverslip onto the cells cultured and treated in a polystyrene/glass confocal dish (BDD011035, JET BIOFIL). Following washing, the fluorescence from the cells was detected to study hypoxia-responsive DOX and shHIF-1α release on a confocal laser scanning microscope (CLSM, TCS SP8, Leica) using DOX (488 nm laser and 560 nm emission) and GFP channels (488 nm laser and 507 nm emission), respectively.

For tumor cell spheroids, MDA-MB-231 cells dispersed in the medium containing Matrigel matrix gel (2.5%, v/v) were added into a 384-well U-bottom plate ($1 \times 10^4$ cell/well), followed by centrifugation (4 °C, 1000 g, 10 min). When growing as uniform sphere, tumor spheroids were treated with different drug formulations (5 μg/mL DOX or its equal volume). After 24 h incubation under normoxia (37 °C, 100% air atmosphere), tumor spheroids were carefully washed with PBS and suctioned to a glass-bottom culture dish for fluorescence observation using CLSM. Tumor spheroids were allowed to attach for 30 min before imaging. With the same treatment protocol, the volume of tumor spheroids was monitored over time. Tumor spheroid volume was calculated as $V = (L \times W^2)/2$, where L and W represented spheroid length and width, respectively.

#### 2.4.4. In vitro silencing efficiency of HIF-1α and its downstream genes

*In vitro* silencing of HIF-1α in protein level was assessed by cell immunofluorescence and western blot. For immunofluorescence, MDA-MB-231 cells were treated with different drug formulations (0.5 μg/mL DOX or its equal volume) under normoxia and hypoxia for 24 h. The cells were then fixed with 4% paraformaldehyde for 20 min, washed twice with PBS, blocked with 10% BSA for 30 min, and sequentially incubated with anti-HIF-1α mouse polyclonal antibody (1:400, MAB1536, R&D Systems,) in PBST overnight, its corresponding donkey anti-mouse secondary antibody conjugated with Alexa Fluor® 647 nm (1:500, AB150107, Abcam) for 1 h, and DAPI for 10 min. After rinsing with PBS, the fluorescence of DAPI and HIF-1α was observed on the CLSM using their corresponding fluorescence filters. For western blot, the treated cells were homogenized with lysis buffer containing protease inhibitor and centrifuged to collect protein. The protein was then quantified using a BCA protein assay kit (Beyotime, Shanghai), separated by electrophoresis with SDS-polyacrylamide gel, and transferred to a PVDF membrane (Millipore, MA). The membrane was blocked in TBST containing 5% milk for 1 h and sequentially incubated in with anti-HIF-1α goat polyclonal antibody (1: 2000, AF1935, R&D Systems) in TBST overnight and donkey anti-goat secondary antibody (1:5000, AB97110, Abcam) for another 1 h. Finally, the sample was detected by enhanced chemiluminescence with β-actin as a control. Western blot was quantified using ImageJ software.

*In vitro* silencing of HIF-1α and its downstream genes, such as vascular endothelial growth factor (VEGF)and matrix metalloproteinase-9 (MMP-9) in mRNA level, was assessed by RT-qPCR. Total RNA was extracted from the treated cells using TRIzol™ (ThermoFisher, MA) and reversed to cDNA by a reverse transcription kit (Vazyme, Nanjing) according to the manufacturer's protocols. RT-qPCR was performed using SYBR Green qPCR Master Mix (MCE, NJ) on a StepOnePlus system (ThermoFisher, MA). The thermocycling conditions were a three-step method with 40 cycles of 60℃ − 72℃ − 60℃. The mRNA fold-change of HIF-1α, VEGF, and MMP-9 was calculated by Livak method and was normalized to β-actin. The primes used were summarized in Supplementary Table S2.

#### 2.4.5. Cell viability and cell migration

Following drug treatment and subsequent incubation under normoxia for 4 h for cell uptake, as described in section 2.4.3, MDA-MB-231 cells were incubated under normoxia or hypoxia for 24 h for cell viability assessment by MTT using an automatic microplate reader (Synergy 2, Bio-TEK). In another experiment, MDA-MB-231 cells cultured and treated in a 6-well plate were scratched using a 1 mL pipette to generate a wound area. After further incubation under normoxia or hypoxia for 24 h, the wounds were observed on an inverted microscope. Cell migration ratio was defined as the reduced wound area at 24 h post-treatment relative to the initial area. The wound area was acquired by ImageJ software. DOX concentrations were 0.05 μg/mL for MTT and 0.5 μg/mL for cell migration. It was noted that DOX concentration used for 3D-cultured tumor spheroids (5 μg/mL) was significantly higher than that for 2D-cultured cell experiments, because tumor spheroids were more tolerable to drug.

### 2.5. Animal experiment

#### 2.5.1. Murine model of orthotopic TNBC

BALB/c nude mice (6 weeks old, female) were supplied by Animal Center of Nantong University and used in accordance with the protocols approved by Animal Care and Use Committee of Nantong University. One hundred microliters of MDA-MB-231 cell suspension ($5 \times 10^7$ cells/mL) placed on ice prior to use were inoculated into the left 4th mammary fat pad of the mice. The mice were then housed in standard cages and given free access to food and water.

#### 2.5.2. Drug treatment

On the 21st day after cell inoculation, tumor-bearing mice were randomly divided and intravenously received drug treatment every three days for a total of five times. DOX dose was 3 mg/kg and corresponding shHIF-1α dose was estimated to be 30 μg/mice. Tumor volume of the mice was monitored every other day and survival situation of the mice was checked every day. Tumor volume was calculated as $V = (L \times W^2)/2$, where L and W represented tumor length and width, respectively.

At 48 h after the last injection, all mice were euthanized and the hearts, livers, spleens, lungs, kidneys, and tumors were harvested for imaging in a small animal dedicated IVIS imaging system (Lumina II, Caliper Life Sciences) to study hypoxia-responsive intratumoral release by monitoring DOX fluorescence. Moreover, harvested tumors were sectioned for immunofluorescence or homogenized for western blot and RT-qPCR to investigate the expression of HIF-1α, VEGF, and MMP-9 in protein and mRNA level according to the protocols described in section 2.4.4.

Harvested tumors as well the lungs with metastatic nodules were

weighed, photographed, and then rinsed with PBS, fixed with paraformaldehyde, embedded in paraffin, and cut into sections for haematoxylin/eosin (H&E) staining or Ki-67 immunohistochemistry. For Ki-67 immunohistochemistry, the sections were incubated with Ki-67 rabbit polyclonal antibody (1:500, 28074–1-AP, Proteintech) overnight, followed by incubation with biotinylated goat anti-rabbit IgG (1:1000, AB6721, Abcam) for 30 min. All images were captured using a Leica DM4000B microscope.

In another experiment, tumor-bearing mice intravenously received drug treatment for only once. At 6 h and 12 h post-injection, the mice were euthanized and some main tissues, including the hearts, liver, spleens, lung, kidneys, and tumors, were harvested and treated to determine DOX tissue distribution by high performance liquid chromatography (HPLC) using the protocol described in our previous work [23].

#### 2.5.3. Safety assessment

At 48 h after the last injection, blood samples were taken from the orbit of treated mice to count white blood cells (WBCs), hemoglobin (HGB), and platelets (PLTs) on an automatic hematology analyzer (BC-2800, Mindray, Shenzhen). Harvested hearts, livers, spleens, and kidneys were weighed for organ index assessment and then sectioned for histopathological examination by H&E staining. Organ index was defined as organ weight relative to body weight.

### 2.6. Statistical analysis

All experiments were performed at least three times. Data were analyzed by GraphPad Prism 8.3 software and presented as mean ± standard deviation (SD). Unpaired student's *t*-test and one-way analysis of variance (ANOVA) test were used to compare two groups and multiple groups, respectively. A *p*-value below 0.05 ($p < 0.05$) was considered significantly different.

## 3. Results and discussion

### 3.1. Synthesis of DOX and shHIF-1α co-loaded hypoxia-responsive micelles

PLL-based cationic copolymers, such as PEG-PLL, have been widely used for the delivery of drug and gene for cancer therapy [26]. However, the high pKa value of PEG-PLL (pKa ≈ 10), resulting in unsuccessful endosomal/lysosomal escape, limits delivery efficiency, especially of gene. One of promising strategies to enhance endosomal/lysosomal escape is grafting other polymer segments onto PEG-PLL to lower pKa value and another strategy is introducing responsive moieties into PEG-PLL, enabling stimuli-responsive release [27]. In this work, we designed PEG-AZO-PLL using AZO as a hypoxia-responsive bridge of PEG and PLL. mPEG-NHS was utilized as starting material and AZO was conjugated with mPEG through the reaction of amino terminal of AZO with NHS terminal of mPEG. Through ring-opening polymerization initiated by the residual amino terminal of AZO, followed by the removal of amino-protecting group, mPEG-AZO-PLL was synthesized. Similarly, mPEG-PLL was also synthesized using mPEG-$NH_2$ as starting material. The detailed synthetic procedures as well as detailed information of synthesized copolymers were presented in our previous work [23].

As amphiphilic copolymers with mPEG and PLL acting as hydrophilic and hydrophobic segments, respectively, mPEG-PLL and mPEG-AZO-PLL could self-assemble in aqueous condition, yielding PMs and AZO-PMs. DLS results showed that blank PMs and AZO-PMs were of 133.7 nm and 143.3 nm, respectively, in hydrodynamic diameter with a narrow size distribution (Supplementary Fig. S1 and Table S3). Introducing rigid AZO slightly increased micelles' size. DLS results also demonstrated that both micelles were highly positively charged, owing to abundant amino groups from branched chain of PLL. Hydrophobic DOX, a classic model drug with fluorescence imaging function, was loaded into micelles during the assembly process of copolymer, yielding PMs/DOX and AZO-PMs/DOX. At the fixed ratio of DOX to copolymer (1:5, w/w), EE% and LC% of PMs/DOX were 71.5% and 12.4%, while they were 74.2% and 12.9%, respectively, for AZO-PMs/DOX. It is noted that although hydrophilic DOX·HCl can also be loaded into micelles, EE% is relatively low (<30%), indicating that DOX is loaded mainly through hydrophobic interaction between DOX and PLL. This result also infers that DOX is positively charged, as DOX·HCl can be successfully loaded into negatively charged micelles through electrostatic interaction [28]. DOX loading partially covered the charge of PLL, leading to the slightly reduced surface charge of PMs/DOX and AZO-PMs/DOX compared with blank micelles. Moreover, it was observed that AZO-PMs/DOX had a slightly higher EE% than PMs/DOX. The possible reason is that rigid AZO impairs compactness of micelles, not only increasing micelles' size but also providing more inner space for DOX loading.

Silencing efficiency of shHIF-1α was strongly dependent on its target sequence. Several shHIF-1α with different target sequences were transfected into HEK-293 T cells using lipofectamine 2000 to validate efficiency. As shown in Fig. 1A-C, all shHIF-1α could be successfully transfected into HEK-293 T cells and silenced HIF-1α overexpressed under hypoxia; especially, shHIF-1α-1067 exhibited a relatively high transfection efficiency and a desired HIF-1α silencing efficiency in protein and mRNA levels, and was thus selected for use. The selected shHIF-1α with negative charge was then electrostatically bound to the surface of micelles. Gel electrophoresis results showed that at 1:10 of shHIF-1α to micelles or a less ratio, all micelles could completely bind shHIF-1α with the bands disappearing from gels [29]. Moreover, AZO-PMs/DOX with reduced positive charge after DOX loading unexpectedly exhibited a high binding efficiency in comparison with blank PMs and AZO-PMs, enabling a complete binding at 1:4 of shHIF-1α to micelles. Similar phenomenon was observed in the repeated experiments. It was speculated that DOX loading altered the structure of micelles, as evidenced by significantly increased hydrodynamic size (Supplementary Table S3), and thus facilitated shHIF-1α binding through spatial interaction. DLS results also revealed that the binding of shHIF-1α had a slight effect on the hydrodynamic size but a considerable effect on the surface charge of micelles. For example, after shHIF-1α binding, the hydrodynamic size of AZO-PMs/DOX + shHIF-1α slightly increased from 179.0 to 192.5 nm, whereas the surface charge remarkably reduced from 33.3 to 18.5 mV, due to charge neutralization effect of shHIF-1α. It was noted that in terms of required amount of shHIF-1α, the ratio of 1:15 was used to synthesize all shHIF-1α single-loaded or co-loaded micelles. Moreover, according to LC% of DOX in micelles, the ratio of shHIF-1α to DOX in AZO-PMs/DOX + shHIF-1α was estimated to be 1:1.9 (w/w). Supplementary Fig. S2 demonstrated that AZO-PMs/DOX + shHIF-1α as well as AZO-PMs/shHIF-1α were of desired serum stability, showing no shHIF-1α dissociation within at least 48 h. TEM image of AZO-PMs/DOX + shHIF-1α was shown in Supplementary Fig. S3.

AZO will undergo bio-reductive cleavage under hypoxia, leading to the detachment of hydrophilic and hydrophobic segments of the copolymer and subsequent disassembly of assembled micelles for concomitant payload release (Fig. 2A). The reductive cleavage of AZO under hypoxia was validated by UV–vis spectra. As shown in Fig. 2B-D, AZO displayed one sharp peak at 392 nm with a shoulder peak around 430 nm and the peaks broadened after incorporated into micelles. After treatment in the hypoxic reductive condition generated by $Na_2S_2O_4$, the two characteristic peaks disappeared, due to the cleavage of AZO. Comparatively, AZO-free PMs had no characteristic peaks and displayed no change after hypoxic treatment. TEM images further demonstrated that PMs could maintain their intact spherical morphology, while intact AZO-PMs were no longer observed after the treatment, evidencing hypoxia-induced disassembly of AZO-PMs (Fig. 2E).

The disassembly of micelles will undoubtedly trigger payload release. The cumulative DOX release profiles showed that DOX release in AZO-PMs/DOX, quantified by DOX fluorescence, was remarkably accelerated after hypoxic treatment, almost approaching a plateau at 6

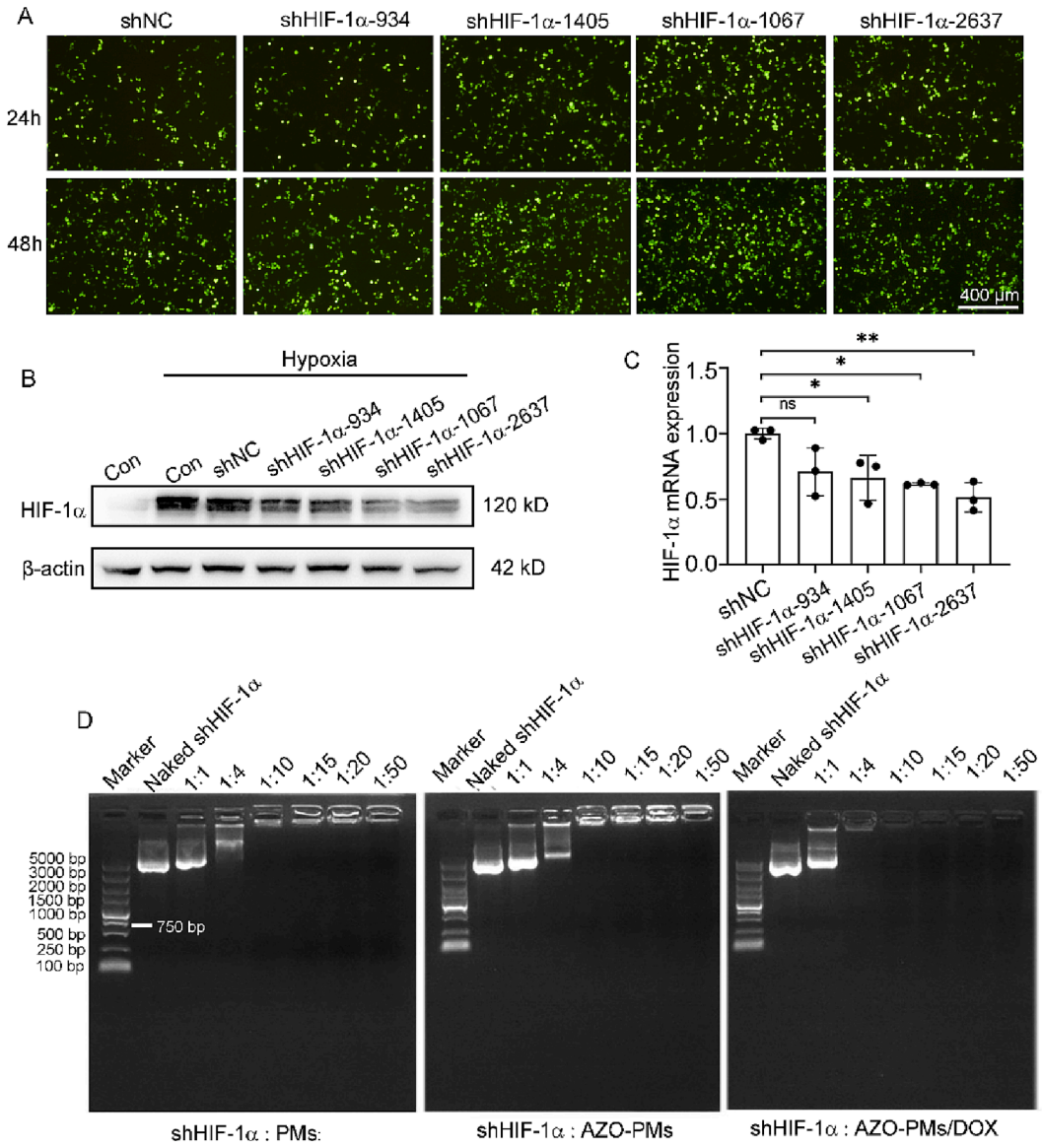


**Fig. 1.** Efficiency validation of shHIF-1α and its binding with micelles. (A) shHIF-1α transfection in HEK-293 T cells using lipofectamine 2000 as vector. HIF-1α silencing efficiency in (B) protein level by western blot and (C) mRNA level by RT-qPCR. (D) The binding of the selected shHIF-1α with PMs, AZO-PMs, and AZO-PMs/DOX in gel electrophoresis in different ratios of shHIF-1α to micelles (w/w). Data were presented as mean ± SD (n = 3). *$p < 0.05$ and **$p < 0.01$.

h, and more than 80% of loaded DOX was released within 24 h; PMs/DOX retained their payload with <20% of loaded DOX released, regardless of treated or not (Fig. 2F). Moreover, AZO-PMs/DOX under normal condition released more DOX than PMs/DOX, according with the hypothesis that the introduction of AZO might impair the compactness of micelles. It was noted that hypoxia-responsive DOX release should be studied with AZO-PMs/DOX + shHIF-1α; however, it was cost-ineffective with a large amount of shHIF-1α needed. Thus, this experiment was only performed with AZO-PMs/DOX. For the same reason, fluorescence quantitation method was not used to study hypoxia-responsive shHIF-1α release, although it was tagged with GFP. Hypoxia-responsive shHIF-1α release was ascertained by gel electrophoresis. As depicted in Fig. 2G, AZO-PMs/DOX + shHIF-1α as well as PMs/shHIF-1α and AZO-PMs/shHIF-1α showed no bands under normal condition, also indicating good binding stability of shHIF-1α with the micelles; after hypoxic treatment, shHIF-1α bands appeared in AZO-PMs/shHIF-1α and AZO-PMs/DOX + shHIF-1α groups, due to shHIF-1α release and movement in the gels in responding to hypoxia. Moreover, AZO-PMs/DOX + shHIF-1α showed almost the same bands with AZO-PMs/shHIF-1α, demonstrating that DOX loading played no considerable role in shHIF-1α dissociation from the micelles, although it facilitated shHIF-1α binding, as discussed above.

### 3.2. *Hypoxia-responsive release augments in vitro antitumor activity of DOX through facilitated delivery and effective silencing of HIF-1α pathway*

All following cell experiments as well as animal experiments were executed in MDA-MB-231 cells, the most studied TNBC cell line. Hypoxia-responsive release was firstly investigated in 2D-cultured cell monolayers under a non-quantitative gradient hypoxia, generated by placing a coverslip on the cells cultured in a confocal dish. While oxygen is continuously consumed by cells, the coverslip prohibits the entering of oxygen, thus generating a gradient hypoxia with oxygen gradually decreasing from the edge to center of the coverslip [23]. CLSM images showed that DOX fluorescence intensity of PMs/DOX remained the same throughout the coverslip, while that of AZO-PMs/DOX increased along with decreased oxygen, indicating that hypoxia-responsive release was highly sensitive. Especially, GFP-tagged shHIF-1α in AZO-PMs/DOX +

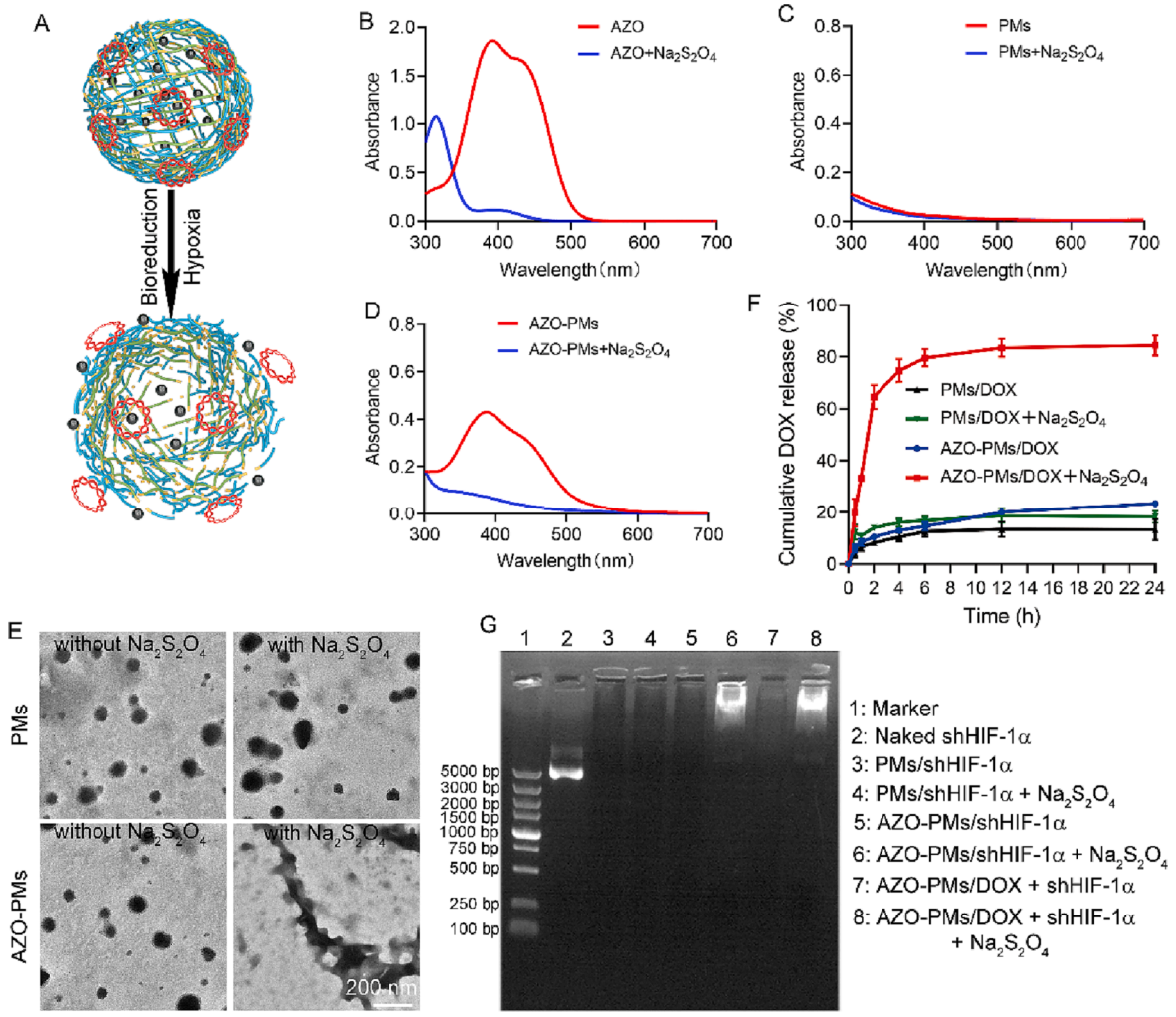


**Fig. 2.** Structural change of hypoxia-responsive micelles for DOX and shHIF-1α release in responding to hypoxia. DOX and shHIF-1α were located in the hydrophobic inner and on the surface of the micelles, respectively. (A) Schematic illustration of the response to hypoxia. UV–vis spectra of (B) AZO, (C) PMs, and (D) AZO-PMs before and after hypoxic treatment. (E) TEM images of PMs and AZO-PMs before and after hypoxic treatment. (F) Cumulative DOX release of PMs/DOX and AZO-PMs/DOX before and after hypoxic treatment. (G) Gel electrophoresis of naked shHIF-1α, PMs/shHIF-1α, AZO-PMs/shHIF-1α, and AZO-PMs/DOX + shHIF-1α. The hypoxic reductive condition was generated by $Na_2S_2O_4$. Data were presented as mean ± SD (n = 3).

shHIF-1α displayed the same release manner with DOX under the gradient hypoxia (Fig. 3A). Hypoxia-responsive release was also investigated under a fixed hypoxia (1% $O_2$). The result further corroborated that hypoxia triggered the release of DOX and shHIF-1α from AZO-PMs (Fig. 3B and 3C). These results generally suggested that AZO-PMs/DOX + shHIF-1α were capable of simultaneously delivering DOX and shHIF-1α to cells through nanoparticle-mediated uptake and simultaneously releasing them in responding to hypoxia, although the payloads were loaded through different mechanisms. As overexpressed azoreductase is necessary to bio-reduce AZO and overexpressed azoreductase is reported to be in the lysosome [30], it is thus deduced that hypoxia-responsive release is triggered in the lysosome, which facilitated lysosomal/endosomal escape for effective delivery, especially of shHIF-1α. This deduction was solidly confirmed by transfection efficiency evaluation. As shown in Fig. 3C and Supplementary Fig. S4, all micelles could successfully transfect shHIF-1α into MDA-MB-231 cells and under hypoxia, AZO-PMs significantly improved shHIF-1α transfection efficiency. Moreover, lipofectamine 2000 was also used to transfect shHIF-1α and however, exhibited a higher toxicity than AZO-PMs with contracted morphology (Supplementary Fig. S5). Generally, PEG-PLL based micelles have the advantages in low cost, good biocompatibility, and flexible decoration for improved transfection efficiency and thus seem to be a more reliable and versatile transfection vector.

Despite various methods developed to fabricate tumor cell spheroids, they cannot perfectly mimic native TME, due to the lack of a number of characteristics of TME, such as high interstitial pressure or microvasculature [31]. On the other hand, tumor spheroids possess some biologically relevant features, including the presence of extracellular matrix, multicellular arrangements, and resultant transport limitation [32,33]. It is reported that transport limitation in tumor spheroids with the diameter larger than 150 μm reduces oxygen diffusion, thus yielding a typical zonation with a normoxic periphery and a hypoxic core [34]. Thus, tumor spheroids can at least partially simulate TME, serving as a powerful *in vitro* model to evaluate tumor penetration and subsequent hypoxia-responsive release. Fig. 3D showed the cross-sectional images of the spheroids exposed to DOX, PMs/DOX, AZO-PMs/DOX, and AZO-PMs/DOX + shHIF-1α with spheroid surface defined as 0 μm. Although free DOX was a small molecule drug, it was unable to deeply penetrate the spheroid and was mainly concentrated at the normoxic periphery. This result was well in accordance with some previous work [35–37]. Loading DOX into micelles could facilitate its penetration into tumor spheroid; however, the general DOX fluorescence intensity in PMs/DOX still remained low throughout the spheroid, due to the shielding effect of micelles. Comparatively, DOX fluorescence in AZO-PMs/DOX was

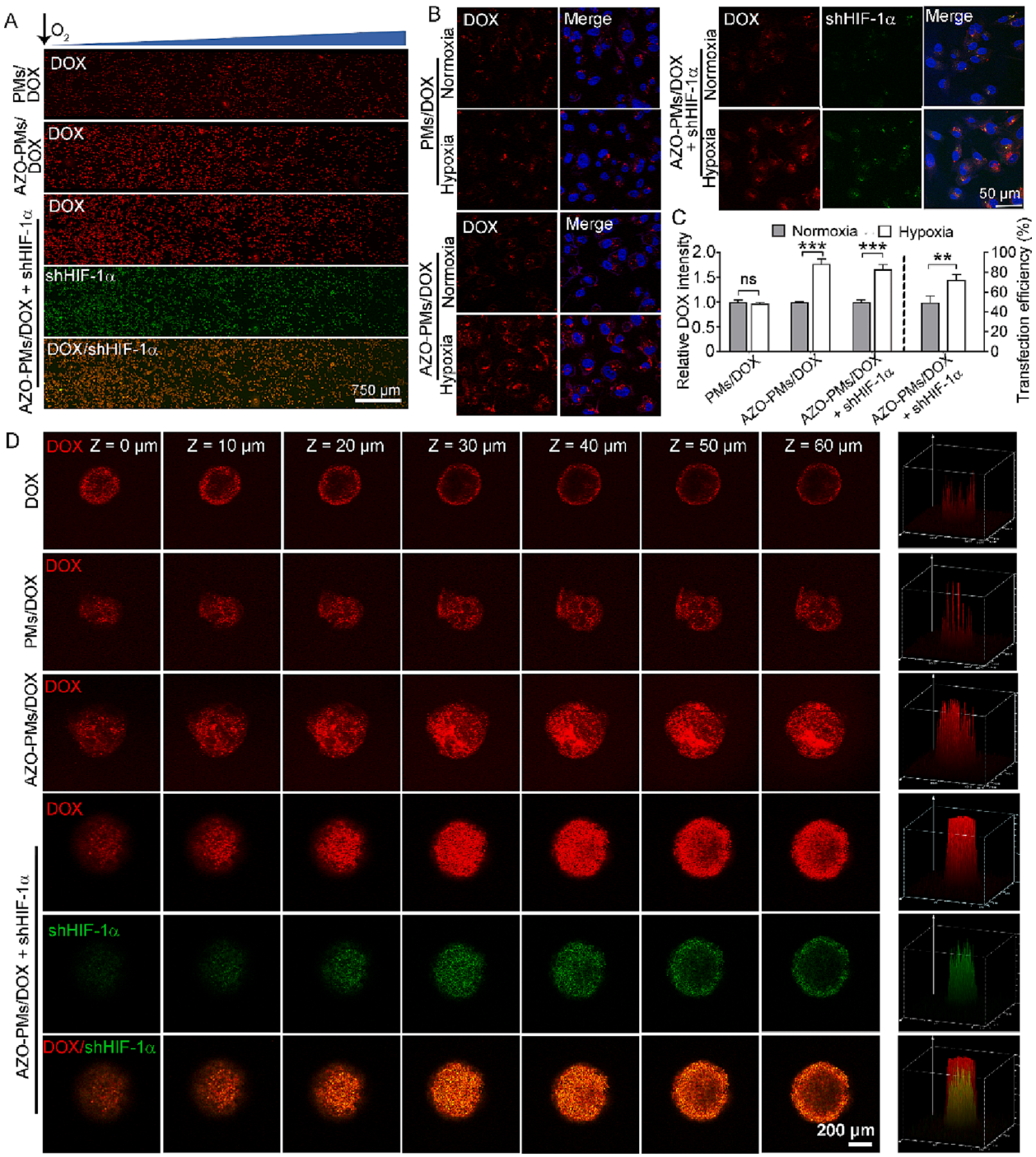


**Fig. 3.** Cell uptake and tumor penetration for hypoxia-responsive release. (A) CLSM observation of hypoxia-responsive release under a non-quantitative gradient hypoxia. (B) CLSM observation of hypoxia-responsive release under normoxia and the fixed hypoxia (1% $O_2$) and (C) quantitative analysis of DOX fluorescence and shHIF-1α transfection efficiency. Transfection efficiency was determined by shHIF-1α fluorescence. (D) Cross-sectional images of 3D-cultured tumor spheroids and corresponding surface plots of images. The cells were treated with DOX, PMs/DOX, AZO-PMs/DOX, and AZO-PMs/DOX + shHIF-1α. DOX concentrations were 0.5 μg/mL and 5 μg/mL for 2D-cultured cells and 3D-cultured tumor spheroids, respectively. Data were presented as mean ± SD (n = 3). $^{**}p < 0.01$ and $^{***}p < 0.001$.

visibly stronger in the hypoxic core than in the normoxic periphery, indicating hypoxia-responsive release. Moreover, it is believed that NDDS just facilitates drug penetration and is still unable to deliver it to the deep core. The fact should be that the micelles to some extent penetrated the spheroids and released DOX in responding to hypoxia, and released DOX diffused inside the spheroids. This speculation could be indirectly verified by the phenomena that strong DOX fluorescence in PMs/DOX was only scattered, while it was relatively concentrated in the core in AZO-PMs/DOX (Fig. 3D). Importantly, AZO-PMs/DOX + shHIF-1α exhibited the strongest DOX fluorescence among all groups with strong DOX and shHIF-1α fluorescence distributed throughout the spheroid. Moreover, DOX fluorescence intensity at the surface of spheroid (z = 0 and 10 μm) was comparable for AZO-PMs/DOX and AZO-PMs/DOX + shHIF-1α and however, in the deep of spheroid (z = 30 and 40 μm), the fluorescence intensity of AZO-PMs/DOX + shHIF-1α was visibly higher than that of AZO-PMs/DOX. This result strongly suggested that effective shHIF-1α delivery could further improve tumor penetration, which would be discussed later.

As AZO-PMs facilitated shHIF-1α delivery under hypoxia, their high efficiency in silencing HIF-1α was predictable. Cell immunofluorescence revealed that HIF-1α was also expressed under normoxia (Supplementary Fig. S6) and was overexpressed under hypoxia. Overexpressed HIF-1α was found to translocate from cytoplasm to nucleus, which probably was an indication of the activation of its downstream genes [38]. PMs/shHIF-1α as a conventional transfection vector could silence overexpressed HIF-1α in protein level and however, the efficiency was unsatisfactory. As expected, AZO-PMs/shHIF-1α exhibited a significantly improved HIF-1α silencing efficiency under hypoxia in comparison with PMs/shHIF-1α (Fig. 4A and B). Western blot also confirmed this result (Fig. 4C and D). Moreover, there was a significantly elevated expression of HIF-1α after treatment with AZO-PMs/DOX + shHIF-1α under hypoxia although such a phenomenon was not observed under normoxia, indicating that DOX might upregulate HIF-1α expression under hypoxia. To verify it, AZO-PMs/DOX group was additionally added in the following RT-qPCR. RT-qPCR results matched cell immunofluorescence and western blot quite well (Fig. 4E). Especially, AZO-PMs/DOX remarkably upregulated HIF-1α expression in mRNA level under hypoxia, contributing to a higher HIF-1α expression of AZO-PMs/DOX + shHIF-1α than that of AZO-PMs/shHIF-1α. The regulation of DOX on HIF-1α expression is found to be conflicting. DOX was used as a HIF-1α inhibitor in some cases [39], while it was reported to upregulate HIF-1α in the most of cases. Despite undetermined cutoff point, which should vary among different cell types, we ascertained that the regulation of DOX on HIF-1α actually depended on DOX concentration, showing an upregulation effect at a low concentration but a silencing effect at a high concentration (data not shown). This finding also suggests that HIF-1α overexpression induced by low-dose DOX treatment might be one of the mechanisms accounting for rapid resistance of hypoxic TNBC to DOX [40]. Vascular endothelial growth factor (VEGF) and matrix metalloproteinase-9 (MMP-9) are the two downstream genes of HIF-1α, which mediate tumor angiogenesis, invasion, and metastasis [41]. RT-qPCR further validated that VEGF and MMP-9 expression was in positive correlation with HIF-1α expression and AZO-PMs/shHIF-1α exhibited the best VEGF and MMP-9 silencing efficiency (Fig. 4F and G). Of course, DOX was also responsible for the elevated VEGF and MMP-9 gene expression in AZO-PMs/DOX + shHIF-1α. These results generally

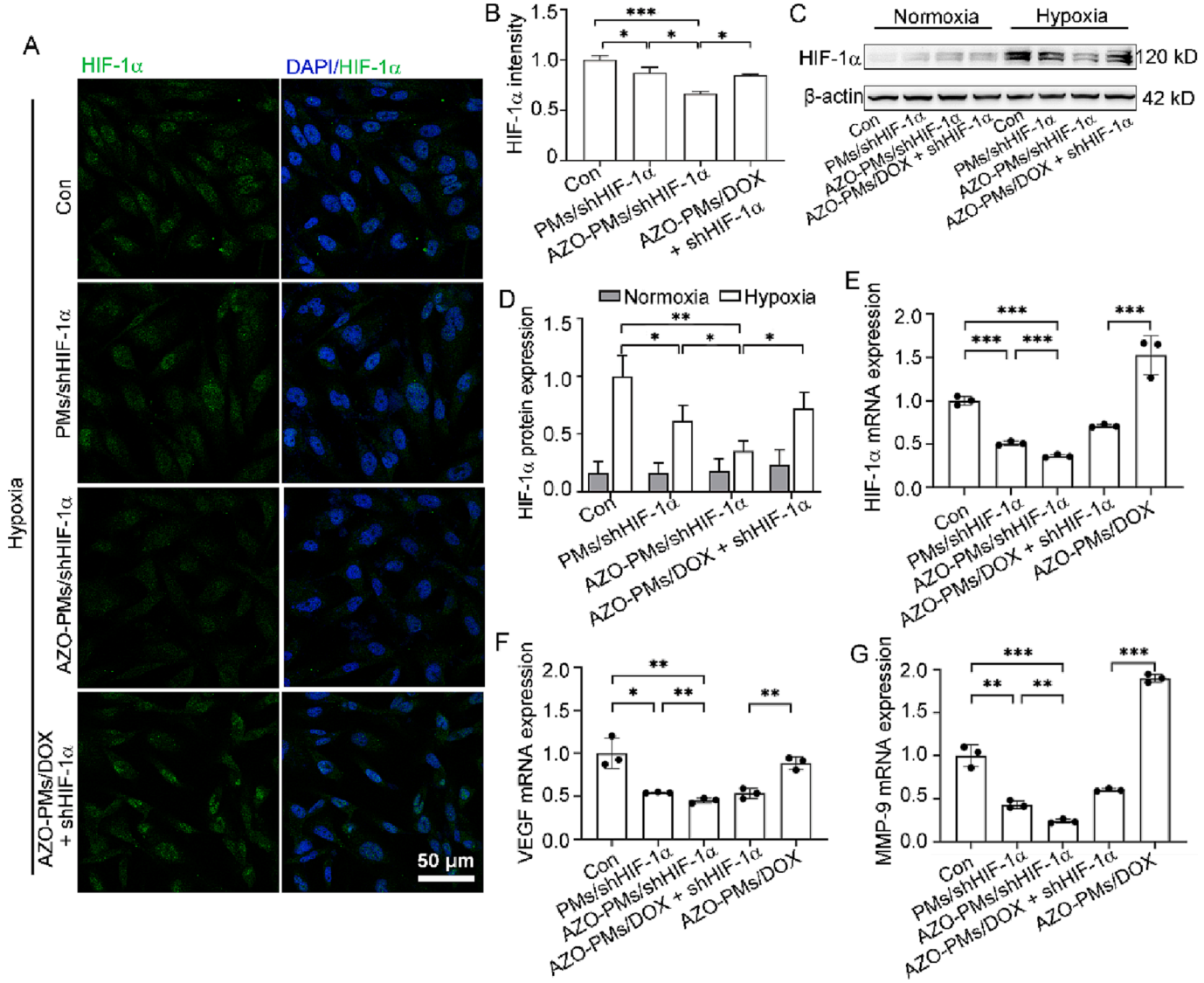


**Fig. 4.** Hypoxia-responsive release for effective silencing of HIF-1α and its downstream genes. (A) HIF-1α expression after treatment under hypoxia by immunofluorescence and (B) corresponding quantitative analysis. (C) HIF-1α expression in protein level after treatment under normoxia and hypoxia by western blot and (D) corresponding quantitative analysis. (E-G) HIF-1α, VEGF, and MMP-9 expression in mRNA level after treatment under hypoxia by RT-qPCR. The cells were treated with PMs/shHIF-1α AZO-PMs/shHIF-1α AZO-PMs/DOX, and AZO-PMs/DOX + shHIF-1α. DOX concentration was 0.5 μg/mL. Data were presented as mean ± SD (n = 3). $^{*}p < 0.05$, $^{**}p < 0.01$, and $^{***}p < 0.001$.

verified that AZO-PMs could facilitate gene delivery for effective silencing of HIF-1α and its downstream genes through sensitive response to hypoxia. Moreover, together with the above result that AZO-PMs/DOX + shHIF-1α had an improved tumor penetration capacity in comparison with AZO-PMs/DOX (Fig. 3D), it was conjectured that silencing HIF-1α and its pathway modulated hypoxic TME and thus greatly facilitated tumor penetration.

HIF-1α is the master regulator of the adaptive response of tumor to hypoxia [42]. A *meta*-analysis of 91 HIF-1α target genes revealed that up to 20 different pathways were regulated by HIF-1α and these pathways interconnect, developing a complex network [43]. Due to interconnected HIF-1α pathways, the functions of HIF-1α are complicated and even opposite in different stages of cancer progression [44], resulting in the clinical results of HIF-1α targeted therapy alone being below expectation. Thus, up to date, there are no approved HIF-1α inhibitors yet. Nonetheless, accumulating evidence has verified that silencing HIF-1α can significantly boost therapeutic outcome of existing treatments [45,46]. Given the vital role of HIF-1α in TNBC, HIF-1α targeted gene therapy in combination with chemotherapy is believed to be promising for the successful treatment of TNBC [47].

*In vitro* antitumor activity of free DOX, PMs/DOX, AZO-PMs/ DOX, and AZO-PMs/DOX + shHIF-1α was first evaluated by MTT. AZO-PMs/DOX + shNC was additionally added as a negative control. MTT assay revealed that the toxicity of AZO-PMs/DOX was equal to that of PMs/DOX under normoxia and was significantly augmented under hypoxia, attributing to hypoxia-responsive release for a high effective dose. Remarkably, while a similar toxicity was observed in AZO-PMs/DOX, AZO-PMs/DOX + shHIF-1α, and AZO-PMs/DOX + shNC under normoxia, AZO-PMs/DOX + shHIF-1α displayed a higher toxicity than the other two groups under hypoxia, strongly identifying that effective HIF-1α silencing sensitized the cells to DOX (Fig. 5A). MTT assay also revealed that the toxicity of blank micelles was neglectable, regardless of normoxia or hypoxia, indicating their good biocompatibility (Supplementary Fig. S7). Wound-healing assay was then carried out to valuate the inhibitory effect of different drug formulations on tumor cell migration, an essential prerequisite for invasion and distant metastasis of tumor cells. The result was well consistent with that in MTT assay and AZO-PMs/DOX + shHIF-1α also significantly inhibited tumor cell migration under hypoxia in comparison with the other formulations (Fig. 5B and C). Improved antitumor activity of AZO-PMs/DOX + shHIF-1α was further ascertained by monitoring the growth of tumor spheroids. As shown in Fig. 5D and E, the spheroid without treatment grew fast over time and PMs/DOX treatment only delayed its growth, despite facilitated tumor penetration. After treatment with AZO-PMs/DOX and AZO-PMs/DOX + shNC, the growth of the spheroids was inhibited, showing a tendency to shrink. As expected, AZO-PMs/DOX + shHIF-1α significantly inhibited the growth of the spheroid in comparison with AZO-PMs/DOX. As a similar antitumor activity was found in AZO-PMs/DOX and AZO-PMs/DOX + shNC, the significantly improved antitumor activity of AZO-PMs/DOX + shHIF-1α in comparison with AZO-PMs/DOX was thus attributed to effective HIF-1α pathway silencing. Generally, by sequentially targeting tumor hypoxia for deep tumor penetration, site-specific and simultaneous release, and effective HIF-1α pathway silencing, AZO-PMs/DOX + shHIF-1α exhibited a desired *in vitro* antitumor activity in treating TNBC cells.

Due to directly acting on cells, free DOX always displays a higher antitumor activity than conventional DOX-loaded NDDS in cell experiments. Herein, the antitumor activity of free DOX was not higher than

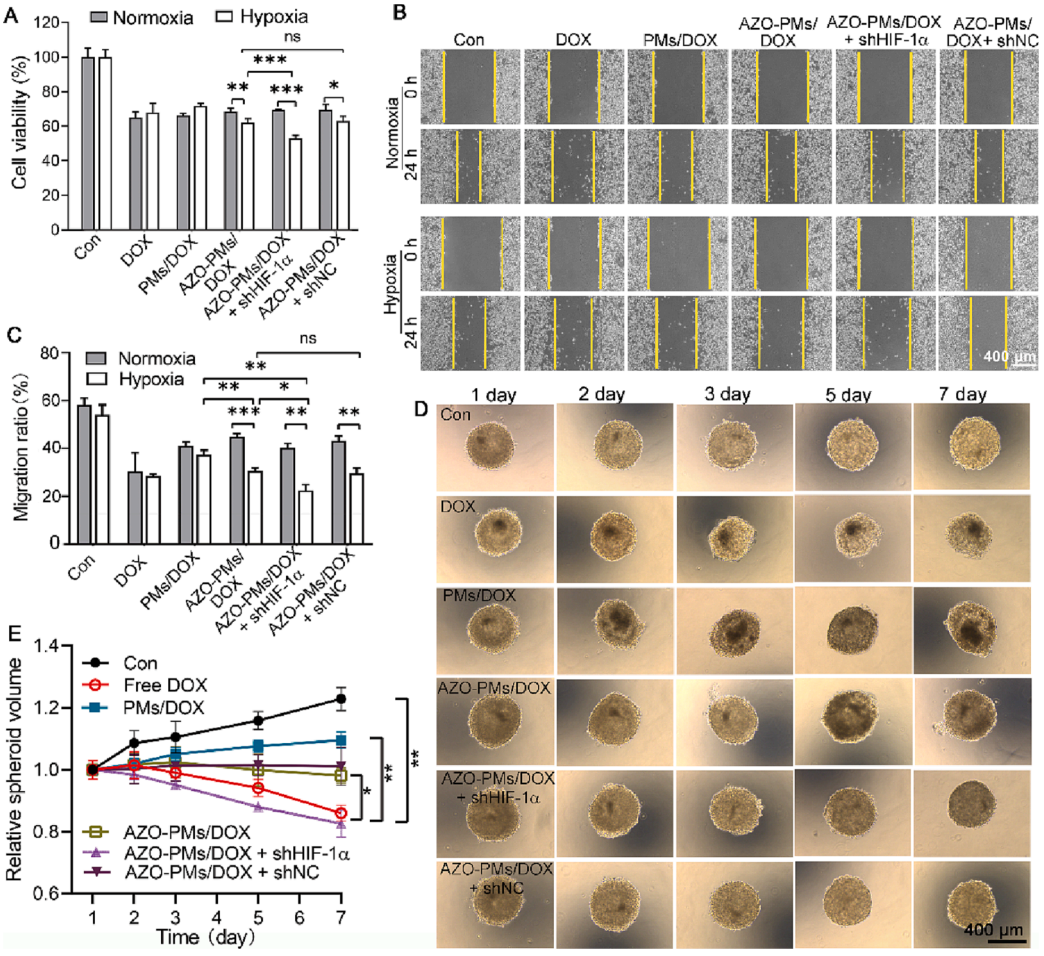


**Fig. 5.** Hypoxia-responsive release in combination with targeted gene therapy for improved antitumor activity. (A) MTT assay after treatment under normoxia and hypoxia. (B) Wound-healing assay after treatment under normoxia and hypoxia and (C) corresponding quantitative analysis of migration ratio. (D) Tumor spheroid growth monitoring and (E) corresponding quantitative analysis of tumor spheroid volume. The cells were treated with DOX, PMs/DOX, AZO-PMs/DOX, AZO-PMs/DOX + shHIF-1α, and AZO-PMs/DOX + shNC. DOX concentrations were 0.05 μg/mL for MTT, 0.5 μg/mL for cell migration, and 5 μg/mL for tumor spheroid. Data were presented as mean ± SD (n = 3 – 6). $^{*}p < 0.05$, $^{**}p < 0.01$, and $^{***}p < 0.001$.

AZO-PMs/DOX under hypoxia, indicating that AZO-PMs as well as PMs actually improved DOX uptake. The uptaken DOX is shielded in the micelles under normoxia for a restricted antitumor activity and is released from AZO-PMs under hypoxia for an improved antitumor activity. Moreover, it was observed that free DOX also significantly inhibited the growth of the spheroid, which was comparable to AZO-PMs/DOX + shHIF-1α. As revealed in Fig. 3D, free DOX was unable to penetrate the spheroid and mainly concentrated at its periphery. In view of this, free DOX should not have such a high inhibitory effect. As tumor cells at the periphery of tumor spheroids is more proliferative than those in the core [48], the possible reason might be that free DOX kills tumor cells with high proliferative potential at the periphery of tumor spheroid, thus remarkably inhibiting its growth. It is worth noting that a relatively high *in vitro* antitumor activity of free DOX cannot predict its *in vivo* antitumor activity, because it has to suffer from poor pharmacokinetic performances before reaching tumor sites.

### 3.3. Hypoxia-responsive intratumoral release facilitates in vivo delivery and silencing of HIF-1α pathway

After tumor-bearing mice intravenously received drug treatment, DOX content in some main tissues, including the hearts, livers, spleens, lungs, kidneys, and tumors, at 6 h and 24 h post-injection was firstly determined to study drug dynamic distribution. It was observed that DOX tissue distribution was improved after being loaded into micelles (Supplementary Fig. S8). Non-specific uptake by macrophages in the reticuloendothelial system contributed to preferential accumulation in the livers and spleens, while the EPR effect facilitated accumulation in tumors. Especially, DOX content of all micellar drug formulations in the normal tissues sharply decreased over time, while it remained high in

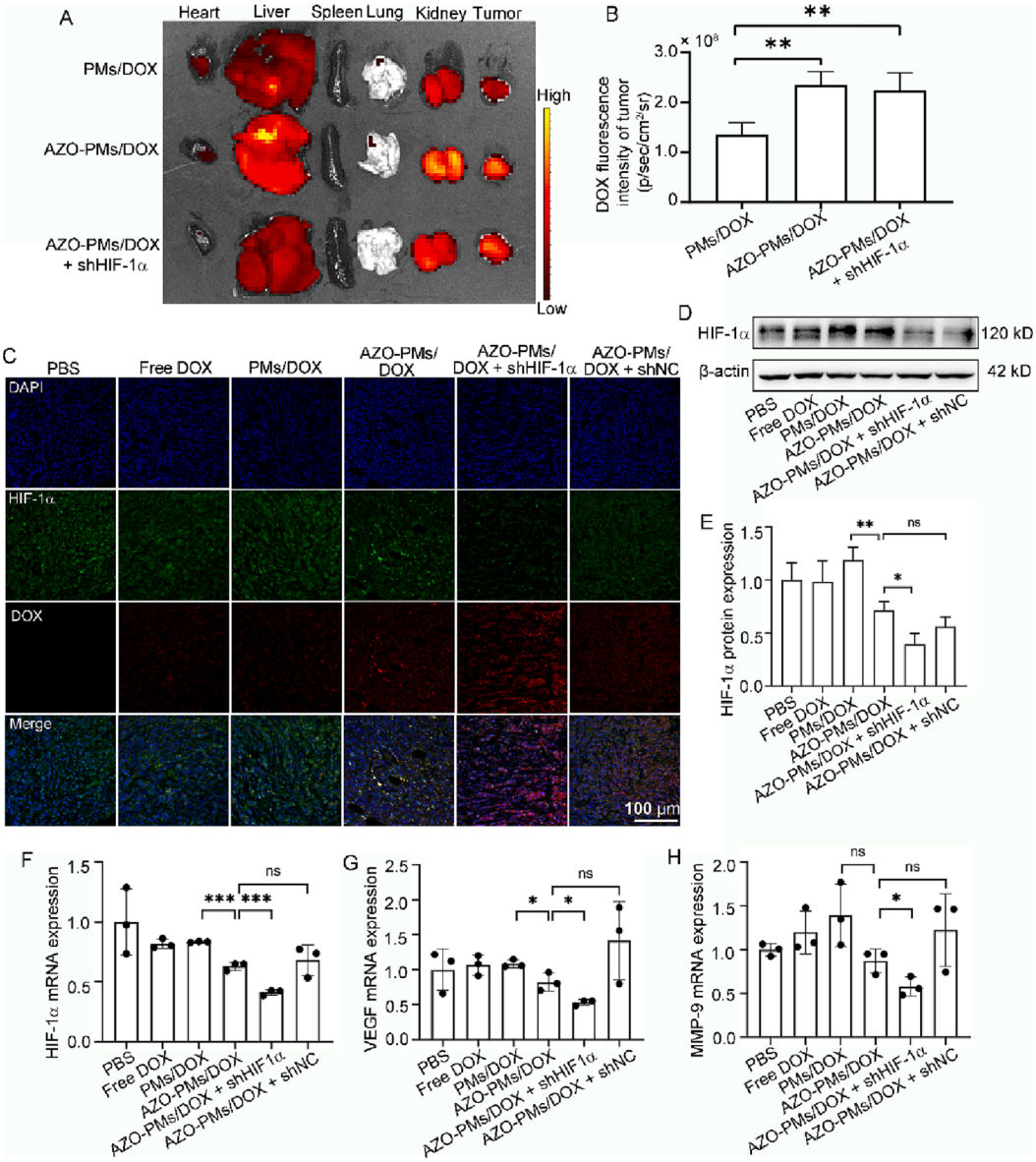


**Fig. 6.** Hypoxia-responsive intratumoral release for effective silencing of HIF-1α and its downstream genes. (A) NIR fluorescence imaging of harvested tissues and (B) corresponding quantitative analysis of DOX fluorescence intensity. (C) HIF-1α expression in tumors by immunofluorescence. (D) HIF-1α expression in protein level in tumors by western blot and (E) corresponding quantitative analysis. (F-H) HIF-1α, VEGF, and MMP-9 expression in mRNA level in tumors by RT-qPCR. Starting from the 21st day after tumor cell inoculation, BALB/c nude mice bearing orthotopic MDA-MD-231 tumor were intravenously treated with PBS, free DOX, PMs/DOX AZO-PMs/DOX, AZO-PMs/DOX + shHIF-1α, and AZO-PMs/DOX + shNC every three days for a total of five times. At 48 h after the last injection, tumors as well as well the hearts, livers, spleens, lungs, and kidneys were harvested for analysis. DOX dose was 3 mg/kg and corresponding shHIF-1α dose was estimated to be 30 μg/mice. Data were presented as mean ± SD (n = 3). $^{*}p < 0.05$, $^{**}p < 0.01$, and $^{***}p < 0.001$.

tumors, indicating the advantage of NDDS in delivering payloads to tumor. No difference in tissue distribution was observed among micellar drug formulations.

In the following, near-infrared-emitting (NIR) fluorescence imaging was carried out to study hypoxia-responsive intratumoral release by monitoring DOX fluorescence. It is noted that DOX is not suitable for real-time *in vivo* fluorescence imaging, attributing to its short-wavelength luminescence being out of NIR window and resultant low signal-to-background ratio [49]. Thus, the main tissues were harvested for *ex vivo* NIR imaging following drug treatment. The results revealed that PMs/DOX, AZO-PMs/DOX, and AZO-PMs/DOX + shHIF-1α exhibited similar DOX fluorescence in the normal tissues, which was generally consistent the result of tissue distribution, determined by HPLC. Importantly, AZO-PMs/DOX as well as AZO-PMs/DOX + shHIF-1α showed stronger DOX fluorescence than PMs/DOX, indicating hypoxia-responsive intratumoral release. We also attempted to observe shHIF-1α distribution by monitoring tagged GFP. However, no GFP fluorescence was found, probably due to its shorter luminescence wavelength than DOX, which was strongly interfered by background autofluorescence.

Hypoxia-responsive intratumoral shHIF-1α release for effective silencing of HIF-1α was validated by immunofluorescence of tumors. Immunofluorescence revealed that HIF-1α was overexpressed in MDA-MB-231 tumor and its expression changed after treatment with free DOX, PMs/DOX or AZO-PMs/DOX, due to the effect from DOX (Fig. 6C). Especially, HIF-1α expression was remarkably inhibited after treatment with AZO-PMs/DOX + shHIF-1α as compared to AZO-PMs/DOX as well as AZO-PMs/DOX + shNC, indicating that hypoxia-responsive intratumoral release greatly benefited HIF-1α silencing. Immunofluorescence result also revealed intratumoral DOX distribution by directly observing DOX fluorescence. Due to its poor pharmacokinetic performance, there was a very low DOX distribution in tumor after treatment with free DOX. As tissue distribution revealed that PMs/DOX, AZO-PMs/DOX, and AZO-PMs/DOX + shHIF-1α had similar distribution in tumors, the higher DOX fluorescence in AZO-PMs/DOX than in PMs/DOX was owing to hypoxia-triggered intratumoral release of accumulated DOX, indicating a high effective drug dose for improved antitumor activity. Particularly, AZO-PMs/DOX + shHIF-1α showed further improved intratumoral DOX fluorescence in comparison with AZO-PMs/DOX as well as AZO-PMs/DOX + shNC, corroborating the result in tumor spheroids that AZO-PMs/DOX + shHIF-1α enabled deep tumor penetration through effective silencing of HIF-1α.

Intratumoral silencing of HIF-1α in protein and mRNA levels was further assessed by western blot and RT-qPCR (Fig. 6D-F). Western blot and RT-qPCR results coincided well with immunofluorescence. As expected, AZO-PMs/DOX + shHIF-1α effectively silenced HIF-1α. Moreover, it was found that HIF-1α expression in protein and mRNA levels in AZO-PMs/DOX group was lower than that in PMs/DOX group, indirectly

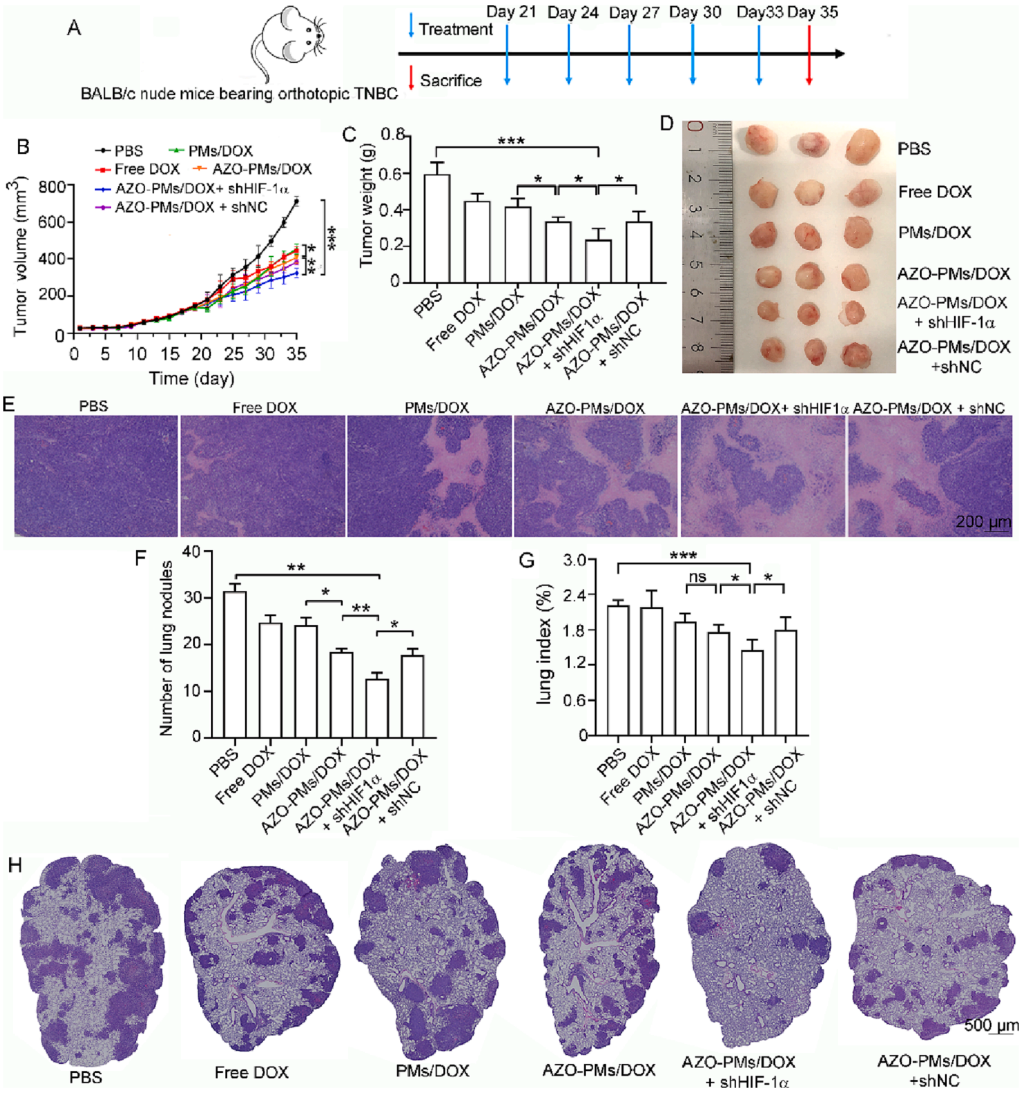


**Fig. 7.** *In vivo* antitumor activity in inhibiting the growth of primary MDA-MB-231 tumor and its distant metastasis to the lung. (A) Protocol of drug treatment for *in vivo* antitumor activity evaluation. (B) Tumor volume monitoring over time. (C) Tumor weight at the end of experimental period and (D) corresponding representative digital images of harvested tumors. (E) H&E staining images of tumor sections. (F) Number of macroscopic metastatic nodules on the surface of the lungs. (G) Lung index assessment by weighing harvested lungs. (H) H&E staining images of the whole lung sections. Data were presented as mean ± SD (n = 3 – 5). $^{*}p < 0.05$, $^{**}p < 0.01$, and $^{***}p < 0.001$.

confirming the above statement that high-concentration DOX down-regulated HIF-1α. Effective silencing of HIF-1α silenced its downstream genes and AZO-PMs/DOX + shHIF-1α thus effectively silenced VEGF and MMP-9, as demonstrated in Fig. 6G and H.

### 3.4. Synergistic chemotherapy and HIF-1α targeted gene therapy inhibit the growth of primary TNBC tumor and its distant metastasis.

To evaluate *in vivo* antitumor activity of different drug formulations in treating TNBC, the mice bearing orthotopic MDA-MD-231 tumor were intravenously treated with PBS, free DOX, PMs/DOX AZO-PMs/DOX, AZO-PMs/DOX + shHIF-1α, and AZO-PMs/DOX + shNC every three days for a total of five times, which started from the 21st day and ended at the 35th day after tumor cell inoculation (Fig. 7A). Fig. 7B revealed that the tumor of PBS group grew fast over time, exceeding 700 $mm^3$ at the end of the experiment, and drug treatment generally delayed tumor growth. Although PMs could improve pharmacokinetic performance of DOX and facilitate its tumor penetration and cell uptake, PMs/DOX only showed parallel antitumor activity to free DOX, due to their inability of rapid release to an effective drug dose. As almost all commercial NDDS is slow-release system, this result solidly corroborates the clinical data that the prominent advantage of conventional NDDS is reduced systemic toxicity but not satisfactory antitumor activity. AZO-PMs/DOX enabled rapid release in responding to hypoxia and thus exhibited significantly improved antitumor activity in comparison with PMs/DOX. While no difference was observed between AZO-PMs/DOX and AZO-PMs/DOX + shNC, AZO-PMs/DOX + shHIF-1α showed further improved antitumor activity, as compared to AZO-PMs/DOX and AZO-PMs/DOX + shNC, indicating that silencing HIF-1α pathway did boost therapeutic outcome of DOX.

At the end of experiment, the tumors were harvested for photographing and weighing. As shown in Fig. 7C and D, tumor weight coincided well with tumor size and AZO-PMs/DOX + shHIF-1α displayed the smallest tumor size and weight among all drug treatment groups. Histopathological feature of the tumors in different groups was evaluated by H&E staining and Ki-67 staining. H&E staining demonstrated that in PBS group, tumor cells showing hyperchromatic nuclei were in highly proliferative status, which packed closely and almost filled tumor stroma. Dead tumor cells were barely found in this group. Free DOX and PMs/DOX inhibited the proliferation of tumor cells, leading to the death of tumor cells for the appearance of some scattered necrotic regions. Necrotic regions were enlarged after treatment with AZO-PMs/DOX and AZO-PMs/DOX + shNC. In particular, AZO-PMs/DOX + shHIF-1α considerably alleviated histological manifestation of tumor with loosely arranged tumor cells and largely enlarged necrotic region occupying a substantial part of the section (Fig. 7E). Ki-67 staining also revealed that AZO-PMs/DOX + shHIF-1α significantly inhibited the proliferation of tumor cells, displaying few Ki-67 positive tumor cells with brown nuclei, as compared to the other treatment groups (Supplementary Fig. S9).

Despite sensitive response of TNBC to systemic chemotherapy, the likelihood of distant metastasis following standard chemotherapy remains high, which causes the vast majority of TNBC-related death. It has been reported that patients with metastatic TNBC will ultimately die of their disease [50]. The lung is the most common site of TNBC metastasis, accounting for up to 70% of metastatic cases [51]. Thus, determining whether a drug formulation can inhibit lung metastasis is of critical importance in evaluating its antitumor activity in TNBC treatment. At the end of experiment, the lungs were also harvested for photographing and weighing. As shown in Supplementary Fig. S10 and Fig. 7F, orthotopic MDA-MB-231 tumor had aggressively metastasized to the lungs, appearing numerous macroscopic metastatic nodules on the surface of the lung in PBS group. Lung metastasis was inhibited after treatment with free DOX and PMs/DOX, which was further inhibited after treatment with AZO-PMs/DOX and AZO-PMs/DOX + shNC. No difference was observed between AZO-PMs/DOX and AZO-PMs/DOX + shNC. As expected, AZO-PMs/DOX + shHIF-1α remarkably inhibited lung metastasis, exhibiting less metastatic nodules than the other treatment groups. Lung index is indicative of lung condition. As healthy lung has a low lung index [52], the relative low value in AZO-PMs/DOX + shHIF-1α group also indicated effective inhibition of lung metastasis (Fig. 7G). Histopathological feature of the lungs in different groups was further evaluated by H&E staining. The result revealed that the lung in PBS group was characterized by a large area of metastatic foci almost occupying half of the section and damaged pulmonary microarchitecture, which resembled lung fibrosis [53], displaying histopathological evidence of lung metastasis. After drug treatment, metastatic area was reduced and especially, AZO-PMs/DOX + shHIF-1α group exhibited the smallest metastatic area with lung microarchitecture appearing regular (Fig. 7H).

It was worth noting that except occasional death in PBS group, no death occurred in all drug treatment groups. However, the mice in some groups looked weak at the late of the experimental period, indicating that they might be suffering from cancer-induced pain, due to aggravated tumor growth and severe distant metastasis. To meet animal ethic requirements as well as avoiding HIF-1α degradation after mice death, all mice were sacrificed ahead of the occurrence of cancer-induced death. Therefore, therapeutic outcome of AZO-PMs/DOX + shHIF-1α in prolonging survival time was unfortunately not well elucidated. Nonetheless, all results verified that by sequentially targeting tumor hypoxia, AZO-PMs/DOX + shHIF-1α was promising in treating TNBC through the following factors: 1) AZO-PMs were capable of deeply penetrating tumor for co-delivery of DOX and shHIF-1α to the hypoxic sites through sensitive response to hypoxic TME, enabling improved antitumor activity of DOX and site-specific silencing of HIF-1α; 2) effective silencing of HIF-1α and its pathway not only ameliorated the response of hypoxic tumor to DOX, but also modulated TME for further improved DOX and shHIF-1α delivery; 3) chemotherapy in combination with HIF-1α targeted gene therapy inhibited the growth of primary TNBC tumor as well as improving TME and consequently, inhibited its distant metastasis; 4) AZO-PMs/DOX + shHIF-1α accumulated in the lung as well as other tissues locally killed metastatic tumor cells.

In spite of cell and organ type-specific function, HIF-1α activity is vital to normal tissue function and development [54]. Possible toxicity caused by systemic treatment with AZO-PMs/DOX + shHIF-1α was our serious concern. Body weight monitoring revealed that compared with free DOX group having a tendency towards weight loss, all the other drug treatment groups maintained their body weight (Supplementary Fig. S11). At the end of the experiment, blood was collected for hematological examination. The result demonstrated that free DOX treatment led to a significant decrease in WBCs and PLTs, as compared to PBS group. No difference was observed among PBS, PMs/DOX and AZO-PMs/DOX groups, indicating that AZO-PMs/DOX were safe. AZO-PMs/DOX + shHIF-1α treatment decreased WBCs and PLTs, although no significant difference was found compared with PBS group (Supplementary Fig. S12). Given a similar decrease of WBCs and PLTs in AZO-PMs/DOX + shNC group, it was concluded that the hematological disorder was owing to high-frequency dosing of pGPU6/GFP/Neo plasmid as vectors of shHIF-1α and shNC but not owing to silencing of HIF-1α. In fact, AZO-PMs/DOX + shHIF-1α could not silence lowly expressed HIF-1α, as verified in Fig. 4C-D and Supplementary Fig. S6. Organ index and H&E staining further demonstrated that AZO-PMs/DOX + shHIF-1α treatment exerted no toxicity to normal tissues (Supplementary Fig. S13 and Fig. S14). These results further suggested that AZO-PMs/DOX + shHIF-1α was safe in treating TNBC.

## 4. Conclusion

In summary, we designed hypoxia-responsive polymeric micelles as the carrier of DOX and shHIF-1α for synergistic chemotherapy and gene therapy of TNBC by sequentially targeting tumor hypoxia. The micelles were readily prepared via self-assembly technique with DOX and shHIF-

1α loaded in their hydrophobic inner and positively charged surface, respectively. The micelles showed high responsive sensitivity, enabling rapid DOX and shHIF-1α release in responding to hypoxia. *In vivo* results further revealed that hypoxia-responsive release could greatly facilitate DOX and shHIF-1α delivery to hypoxic sites, which not only improved antitumor activity of DOX but also effectively silenced HIF-1α pathway activated under hypoxia. As a result, the micelles inhibited the growth of primary TNBC tumor and its distant metastasis in a murine model of orthotopic TNBC, achieved by modulated hypoxic TME and thus further maximized therapeutic outcome of DOX. Together with safety assessment that systemic HIF-1α regulation did not cause remarkable toxicity, synergistic treatment of chemotherapy and HIF-1α targeted gene therapy using hypoxia-responsive NDDS is particularly promising in treating TNBC as well as other hypoxic tumors. Moreover, although clinical application of hypoxia-responsive NDDS remains far away from realization, it shows translational potential in effective *in vivo* delivery of interesting genes involved in hypoxic diseases for the purpose of scientific research.

## Declaration of Competing Interest

The authors declare that they have no known competing financial interests or personal relationships that could have appeared to influence the work reported in this paper.

## Data availability

Data will be made available on request.

## Acknowledgments

The work was supported by the National Natural Science Foundation of China (32271228, 82271914, and 81971131).

## Appendix A. Supplementary data

Supplementary data to this article can be found online at https://doi.org/10.1016/j.cej.2023.144271.

## References

[1] R.L. Siegel, K.D. Miller, H.E. Fuchs, A. Jemal, Cancer statistics, 2022, CA Cancer J. Clin. 72 (2022) 7.
[2] P. Peng, J.-Y. Chen, Y.-T. Han, X. Chen, H.-Y. Li, C.-H. Hu, J.-L. Wang, Impact of surgery on survival in breast cancer with bone metastases only: a SEER database retrospective analysis, BMC Surg. 21 (2021) 378.
[3] L. Yin, J.-J. Duan, X.-W. Bian, S.-C. Yu, Triple-negative breast cancer molecular subtyping and treatment progress, Breast Cancer Res. 22 (2020) 61.
[4] R.L. Copeland, Y. Kanaan, New targets in triple-negative breast cancer, Nat. Rev. Cancer 21 (2021) 744.
[5] S. Harborg, R. Zachariae, J. Olsen, M. Johannsen, D. Cronin-Fenton, H. Bøggild, S. Borgquist, Overweight and prognosis in triple-negative breast cancer patients: a systematic review and meta-analysis, npj, Breast Cancer 7 (2021) 119.
[6] K. Clifton, A. Gutierrez-Barrera, J. Ma, R. Bassett, J. Litton, H. Kuerer, S. Moulder, C. Albarracin, G. Hortobagyi, B. Arun, Adjuvant versus neoadjuvant chemotherapy in triple-negative breast cancer patients with BRCA mutations, Breast Cancer Res. Treat. 170 (2018) 101.
[7] A. Bandyopadhyay, L. Wang, J. Agyin, Y. Tang, S. Lin, I.T. Yeh, K. De, L.-Z. Sun, Doxorubicin in combination with a small TGFβ inhibitor: a potential novel therapy for metastatic breast cancer in mouse models, PLoS One 5 (2010) e10365.
[8] V.M. Khot, A.B. Salunkhe, S. Pricl, J. Bauer, N.D. Thorat, H. Townley, Nanomedicine-driven molecular targeting, drug delivery, and therapeutic approaches to cancer chemoresistance, Drug Discov. Today 26 (2021) 724.
[9] B. Zhang, Y. Hu, Z. Pang, Modulating the tumor microenvironment to enhance tumor nanomedicine delivery, Front. Pharmacol. 8 (2017) 952.
[10] Q.-V. Le, J. Suh, Y.-K. Oh, Nanomaterial-based modulation of tumor microenvironments for enhancing chemo/immunotherapy, AAPS J. 21 (2019) 64.
[11] F. Peng, R. Li, F. Zhang, L. Qin, G. Ling, P. Zhang, Potential drug delivery nanosystems for improving tumor penetration, Eur. J. Pharm. Biopharm. 151 (2020) 220.
[12] Y. Feng, Z. Liao, H. Zhang, X. Xie, F. You, X. Liao, C. Wu, W. Zhang, H. Yang, Y. Liu, Emerging nanomedicines strategies focused on tumor microenvironment against cancer recurrence and metastasis, Chem. Eng. J. 452 (2023), 139506.
[13] W. Zhou, X. Ma, J. Wang, X. Xu, O. Koivisto, J. Feng, T. Viitala, H. Zhang, Co-delivery CPT and PTX prodrug with a photo/thermo-responsive nanoplatform for triple-negative breast cancer therapy, Smart Med. 1 (2022) e20220036.
[14] S. Ghosh, A. Javia, S. Shetty, D. Bardoliwala, K. Maiti, S. Banerjee, A. Khopade, A. Misra, K. Sawant, S. Bhowmick, Triple negative breast cancer and non-small cell lung cancer: clinical challenges and nano-formulation approaches, J. Control. Release 337 (2021) 27.
[15] X. Xie, T. Song, Y. Feng, H. Zhang, G. Yang, C. Wu, F. You, Y. Liu, H. Yang, Nanotechnology-based multifunctional vaccines for cancer immunotherapy, Chem. Eng. J. 437 (2022), 135505.
[16] Y. Wang, X. Ma, W. Zhou, C. Liu, H. Zhang, Reregulated mitochondrial dysfunction reverses cisplatin resistance microenvironment in colorectal cancer, Smart Med. 1 (2022) e20220013.
[17] M.J. Mitchell, M.M. Billingsley, R.M. Haley, M.E. Wechsler, N.A. Peppas, R. Langer, Engineering precision nanoparticles for drug delivery, Nat. Rev. Drug Discov. 20 (2021) 101.
[18] M. Souri, M. Soltani, F. Moradi Kashkooli, M. Kiani Shahvandi, Engineered strategies to enhance tumor penetration of drug-loaded nanoparticles, J. Control. Release 341 (2022) 227.
[19] M. Akman, D.C. Belisario, I.C. Salaroglio, J. Kopecka, M. Donadelli, E. De Smaele, C. Riganti, Hypoxia, endoplasmic reticulum stress and chemoresistance: dangerous liaisons, J. Exp. Clin. Cancer Res. 40 (2021) 28.
[20] X.X. Xu, S.Y. Chen, N.B. Yi, X. Li, S.L. Chen, Z. Lei, D.B. Cheng, T. Sun, Research progress on tumor hypoxia-associative nanomedicine, J. Control. Release 350 (2022) 829.
[21] Y. Li, A. Lu, M. Long, L. Cui, Z. Chen, L. Zhu, Nitroimidazole derivative incorporated liposomes for hypoxia-triggered drug delivery and enhanced therapeutic efficacy in patient-derived tumor xenografts, Acta Biomater. 83 (2019) 334.
[22] M.M. Long, A.L. Lu, M. Lu, L.Y. Weng, Q.P. Chen, L. Zhu, Z.P. Chen, Azo-inserted responsive hybrid liposomes for hypoxia-specific drug delivery, Acta Biomater. 115 (2020) 343.
[23] M.M. Long, X.M. Liu, X.L. Huang, M. Lu, X.M. Wu, L.Y. Weng, Q.P. Chen, X. T. Wang, L. Zhu, Z.P. Chen, Alendronate-functionalized hypoxia-responsive polymeric micelles for targeted therapy of bone metastatic prostate cancer, J. Control. Release 334 (2021) 303.
[24] M. Lu, X. Huang, X. Cai, J. Sun, X. Liu, L. Weng, L. Zhu, Q. Luo, Z. Chen, Hypoxia-responsive stereocomplex polymeric micelles with improved drug loading inhibit breast cancer metastasis in an orthotopic murine model, Acs Appl. Mater. Inter. 14 (2022) 20551.
[25] Q. Liu, C. Guan, C. Liu, H. Li, J. Wu, C. Sun, Targeting hypoxia-inducible factor-1alpha: a new strategy for triple-negative breast cancer therapy, Biomed. Pharmacother. 156 (2022), 113861.
[26] H. Zhu, R. Liu, Y. Shang, L. Sun, Polylysine complexes and their biomedical applications, Eng. Regen. 4 (2023) 20.
[27] N.A. Patil, B. Kandasubramanian, Functionalized polylysine biomaterials for advanced medical applications: a review, Eur. Polym. J. 146 (2021), 110248.
[28] L.P. Sadowski, A. Singh, D.H. Luo, M.J. Majcher, I. Urosev, M. Rothenbroker, V. Kapishon, N.M.B. Smeets, T. Hoare, Functionalized poly(oligo(lactic acid) methacrylate)-block-poly(oligo(ethylene glycol) methacrylate) block copolymers: a synthetically tunable analogue to PLA-PEG for fabricating drug-loaded nanoparticles, Eur. Polym. J. 177 (2022), 111443.
[29] C. Wang, Q. Liu, Z. Zhang, Y. Wang, Y. Zheng, J. Hao, X. Zhao, Y. Liu, L. Shi, Tumor targeted delivery of siRNA by a nano-scale quaternary polyplex for cancer treatment, Chem. Eng. J. 425 (2021), 130590.
[30] C. Zhu, Z. Zou, C. Huang, J. Zheng, N. Liu, J. Li, R. Yang, Highly selective imaging of lysosomal azoreductase under hypoxia using pH-regulated and target-activated fluorescent nanoprobes, Chem. Commun. 55 (2019) 3235.
[31] C. Shao, J. Chi, H. Zhang, Q. Fan, Y. Zhao, F. Ye, Development of cell spheroids by advanced technologies, Advanced Materials Technologies 5 (2020) 2000183.
[32] G. Mehta, A.Y. Hsiao, M. Ingram, G.D. Luker, S. Takayama, Opportunities and challenges for use of tumor spheroids as models to test drug delivery and efficacy, J. Control. Release 164 (2012) 192.
[33] S. Qian, J. Mao, Z. Liu, B. Zhao, Q. Zhao, B. Lu, L. Zhang, X. Mao, L. Cheng, W. Cui, Y. Zhang, X. Sun, Stem cells for organoids, Smart Med. 1 (2022) e20220007.
[34] M. Chatzinikolaidou, Cell spheroids: the new frontiers in in vitro models for cancer drug validation, Drug Discov. Today 21 (2016) 1553.
[35] Z. Xie, W. Guo, N. Guo, M. Huangfu, H. Liu, M. Lin, W. Xu, J. Chen, T. Wang, Q. Wei, M. Han, J. Gao, Targeting tumor hypoxia with stimulus-responsive nanocarriers in overcoming drug resistance and monitoring anticancer efficacy, Acta Biomater. 71 (2018) 351.
[36] S.M. Sagnella, H. Duong, A. MacMillan, C. Boyer, R. Whan, J.A. McCarroll, T. P. Davis, M. Kavallaris, Dextran-based doxorubicin nanocarriers with improved tumor penetration, Biomacromolecules 15 (2014) 262.
[37] J. Liu, C. Chen, T. Wei, O. Gayet, C. Loncle, L. Borge, N. Dusetti, X. Ma, D. Marson, E. Laurini, S. Pricl, Z. Gu, J. Iovanna, L. Peng, X.-J. Liang, Dendrimeric nanosystem consistently circumvents heterogeneous drug response and resistance in pancreatic cancer, Exploration 1 (2021) 21.
[38] J. Yan, X. Huang, D. Zhu, Y. Lou, Enhanced aerobic glycolysis by S-nitrosoglutathione via HIF-1α associated GLUT1/aldolase A axis in human endothelial cells, J. Cell. Biochem. 118 (2017) 2443.
[39] M. Moussa, S.N. Goldberg, G. Kumar, R.R. Sawant, T. Levchenko, V.P. Torchilin, M. Ahmed, Nanodrug-enhanced radiofrequency tumor ablation: effect of micellar or liposomal carrier on drug delivery and treatment efficacy, PLoS One 9 (2014) e102727.

[40] X. Bai, Y. Zhou, Q. Lin, C.K. Huang, S. Zhang, R.I. Carlson, H. Ghanbari, B. Sun, J. R. Wands, X. Dong, Bio-nanoparticle based therapeutic vaccine induces immunogenic response against triple negative breast cancer, Am. J. Cancer Res. 11 (2021) 4141.
[41] J. Fan, B. Liu, Y. Long, Z. Wang, C. Tong, W. Wang, P. You, X. Liu, Sequentially-targeted biomimetic nano drug system for triple-negative breast cancer ablation and lung metastasis inhibition, Acta Biomater. 113 (2020) 554.
[42] C.-C.-L. Wong, D.M. Gilkes, H. Zhang, J. Chen, H. Wei, P. Chaturvedi, S.I. Fraley, C.-M. Wong, U.-S. Khoo, I.-O.-L. Ng, D. Wirtz, G.L. Semenza, Hypoxia-inducible factor 1 is a master regulator of breast cancer metastatic niche formation, Proc. Natl. Acad. Sci. U. S. A. 108 (2011) 16369.
[43] L. Slemc, T. Kunej, Transcription factor HIF1A: downstream targets, associated pathways, polymorphic hypoxia response element (HRE) sites, and initiative for standardization of reporting in scientific literature, Tumor Biol. 37 (2016) 14851.
[44] M. Rashid, L.R. Zadeh, B. Baradaran, O. Molavi, Z. Ghesmati, M. Sabzichi, F. Ramezani, Up-down regulation of HIF-1α in cancer progression, Gene 798 (2021), 145796.
[45] X. Zhang, C. He, G. Xiang, Engineering nanomedicines to inhibit hypoxia-inducible Factor-1 for cancer therapy, Cancer Lett. 530 (2022) 110.
[46] S. Eljack, S. David, A. Faggad, I. Chourpa, E. Allard-Vannier, Nanoparticles design considerations to co-deliver nucleic acids and anti-cancer drugs for chemoresistance reversal, Int. J. Pharm. X 4 (2022), 100126.
[47] Y. Zhang, H. Zhang, M. Wang, T. Schmid, Z. Xin, L. Kozhuharova, W.-K. Yu, Y. Huang, F. Cai, E. Biskup, Hypoxia in breast cancer—scientific translation to therapeutic and diagnostic clinical applications, Front. Oncol. 11 (2021), 652266.
[48] C.R. Thoma, M. Zimmermann, I. Agarkova, J.M. Kelm, W. Krek, 3D cell culture systems modeling tumor growth determinants in cancer target discovery, Adv. Drug Del. Rev. 69–70 (2014) 29.
[49] R. Weissleder, A clearer vision for in vivo imaging, Nat. Biotechnol. 19 (2001) 316.
[50] G. Bianchini, J.M. Balko, I.A. Mayer, M.E. Sanders, L. Gianni, Triple-negative breast cancer: challenges and opportunities of a heterogeneous disease, Nat Rev Clin Oncol 13 (2016) 674.
[51] J.M. Reese, E.S. Bruinsma, A.W. Nelson, I. Chernukhin, J.S. Carroll, Y. Li, M. Subramaniam, V.J. Suman, V. Negron, D.G. Monroe, J.N. Ingle, M.P. Goetz, J. R. Hawse, ERβ-mediated induction of cystatins results in suppression of TGFβ signaling and inhibition of triple-negative breast cancer metastasis, Proc. Natl. Acad. Sci. U. S. A. 115 (2018) E9580.
[52] L. Sun, M. Fan, D. Huang, B. Li, R. Xu, F. Gao, Y. Chen, Clodronate-loaded liposomal and fibroblast-derived exosomal hybrid system for enhanced drug delivery to pulmonary fibrosis, Biomaterials 271 (2021), 120761.
[53] M.-Y. Yang, Y.-J. Lin, M.-M. Han, Y.-Y. Bi, X.-Y. He, L. Xing, J.-H. Jeong, T.-J. Zhou, H.-L. Jiang, Pathological collagen targeting and penetrating liposomes for idiopathic pulmonary fibrosis therapy, J. Control. Release 351 (2022) 623.
[54] Y. Ono, H. Sensui, Y. Sakamoto, R. Nagatomi, Knockdown of hypoxia-inducible factor-1α by siRNA inhibits C2C12 myoblast differentiation, J. Cell. Biochem. 98 (2006) 642.